Thesis for Master Degree

Preliminary Study on Spring Season Daytime Sea Fog Detection Method Using MODIS in the Yellow Sea

Advisor: Prof. Chan-Su Yang

Prof. Young-Su Park

August 2016

Department of Convergence Study on the Ocean Science and Technology
School of Ocean Science and Technology
Korea Maritime and Ocean University

Joo-Young Jeon

Approved by the Committee of the Ocean Science and Technology School of Korea Maritime and Ocean University in Fulfillment of the Requirements for the Degree of Master's in Engineering

Prof. Eun-Bang Lee, Chair ________________

Prof. Chan-Su Yang, Advisor ______________

Dr. Sun-Hwa Kim, Advisor ________________

June 1, 2016

Department of Convergence Study on the Ocean Science and Technology
Ocean Science and Technology School
Korea Maritime and Ocean University

Contents

List of Tables

List of Figures

MODIS 영상을 이용한 봄철 황해지역의 주간 해무탐지 기법 개선 기초연구

전주영

해양과학기술융합학과
한국해양대학교 해양과학기술전문대학원

요약

해무는 봄철과 여름철에 매우 빈번히 발생하고, 이는 낮은 시정으로 해양사고를 유발하여 해양 안전을 위협하는 위험한 요소라 할 수 있다. 최근 해양 활동이 더욱 활성화되면서 해양 안전이 더욱 요구되므로 해무 탐지 결과는 제공되어야 할 필요성이 있다. 이때 지구 상공 위에서 관측되는 위성 데이터를 사용하면 해무의 시・공간적 정보를 제공할 수 있는 장점이 있다.

위성 데이터 중 NASA에서 지구 관측 목적으로 발사된 Terra 위성과 Aqua 위성에 탑재되어있는 Moderate Resolution Imaging Spectroradiometer, MODIS 데이터를 사용하여 주간에 발생된 해무는 False color 로 합성한 칼라 합성영상(color composite image)을 사용하여 수동으로 해무를 탐지될 수 있다. 매번 수동으로 탐지하게되면 정확도는 높지만 천리안 해양관측위성탑재체 (Geostationary Ocean Color Imager, GOCI) 로 관측된 영상이나 천리안 기상관측탑재체 (Meteorological Imager)의 fog product와 같은 참고 자료 또한 함께 동반되어야 하는 불편함이 있고 개인마다 탐지결과가 달라질 수도 있는 객관적인 탐지가 아닐 수도 있다는 단점이 있다. 알고리즘으로 탐지된 해무는 이와 같은 문제를 해소할 수 있다.

본 연구에서 발표한 알고리즘은 기존의 MODIS 해무탐지 알고리즘에서 활용한 Terra/MODIS 뿐만 아니라 Aqua/MODIS 에도 적용할 수 있는 알고리즘으로 우리나라 해역과 봄철에 발생하는 해무 탐지의 정확도를 개선하기 위해 해무나 다른 구름들의 물리적 특성에 따라 각 채널에 얻어지는 분광특성을 활용하여, Normalized Difference Snow Index(NDSI), 표준편차 테스트

(Standard deviation, STD test), 운정 밝기온도와 해수면온도의 차로 얻어진 Temperature difference index(TDI), Normalized near-infrared water vapor index(NWVI) 와 같은 여러 인덱스에 황해와 봄철에 맞는 임계값을 순차적으로 적용하여 탐지할 수 있어 이전의 연구보다 더 높은 정확도로 주간해무가 가능하다.

우리나라 인근해역에서 황해 봄철에 많은 해무가 발생하였고, 이에 봄철 황해에 발생한 아홉가지의 해무 케이스를 training data로 사용하면서 각 인덱스의 임계값을 수동 탐지 결과와 알고리즘 탐지 결과를 Hanssen-Kuiper Skill Score(KSS)를 사용하여 결정하였다. 기 개발된 알고리즘에 비하여 본 알고리즘은 Terra 와 Aqua 자료 모두 사용가능하며, 황해와 봄철에 발생하는 해무에 최적화되어있는 임계값을 제시한다. 또한 1 km의 높은 해상도 SST 자료를 사용하면서 탐지 정확성을 더욱 정밀하게 높일 수 있다. 검증 데이터를 개선된 알고리즘에 적용했을 때 해무탐지 결과는 0.72 KSS 값을 나타내며 이는 기 개발된 알고리즘을 사용한 결과보다 더 높은 해무 탐지 가능성을 보여준다.

KEY WORDS: Sea fog, MODIS, Threshold scheme, Yellow Sea, Hanssen-Kuiper Skill Score

Chapter 1. Introduction

1.1 Background

Sea fog is a dangerous meterological phenomenon that causes lots of marine accident due to poor visibility (Heo et al., 2008). The statistics from Korean Maritime Safety Tribunal show that 29.5% of marine accidents were occurred during sea fog events (KMST, http://www.kmst.go.kr). The monitoring of sea fog can contribute in managing the traffic and ensuring the safety at sea. However forecasting/nowcasting of sea fog still remain unsolved because of the characteristics of temporal and spatial variability of fog (Gultepe et al., 2007). Also due to its physical problems, there are only limited observation stations in ocean (Cermack and Bendix, 2007). Using remote sensing technology, sea fog can be detected with high spatial and temporal resolution (Ellrod, 1995; Ahn et al., 2003; Yoo et al., 2005; Heo et al., 2008). It is possible to monitor sea fog effectively using satellite data with wide coverage from the space.

Currently in Korea, fog related information are provided in visibility which are observed from weather stations in the nation. Alternatively, it is provided with fog product produced by Meteorological Imager (MI) which is loaded on Communication, Ocean and Meteorological Satellite (COMS). The National Meteorological Satellite Center provides fog product of Korean Peninsula region and East Asia region observed using MI with interval of 15 minutes in resolution of 4 km (http://nmsc.kma.go.kr/html/homepage/en/satellite/searchSatelliteImageN.do?data_type=1095).

Many previous studies attempted to detect sea fog using various satellite data with various methods such as the Moderate-resolution Imaging SepectroRadiometer (MODIS) (Bendix et al., 2005; Zhang and Yi, 2013; Wu and

Li, 2014; Dong et al., 2015), Advanced very-high-resolution radiometer, AVHRR (Eyre et al., 1984; Bendix, 2002; Heo et al., 2008), Geostationary Operational Environmental Satellite, GOES (Ellord, 1995; Lee et al., 1997; Bendix, 2002) Multi-functional Transport Satellite, MTSAT (Heo et al., 2008; Park et al., 2012).

Among many sensors loaded on many other satellites, the MODIS loaded on Terra and Aqua satellites has wide spectral range from 0.4 μm to 14 μm for with 36 spectral bands, or groups of wavelengths (Table 1). MODIS is developed from NASA for Earth Observing System, EOS project. Terra MODIS and Aqua MODIS are observing the entire Earth's surface once or twice every day. The detail description of Terra and Aqua is described in Table 2. The Geostationary Ocean Color Imager (GOCI) provides higher temporal resolution with eight scenes every day from 00:15 to 07:15 (UTC). However it only has visible and near-infrared (NIR) channels which mean it is not capable of adapting the detection methods that has been presented so far. On the other hand, MODIS provides with the wide spectral range which provides more capability of developing sea fog detection method compare to other spectrometer (Gultepe et al., 2007).

In the Yellow Sea, sea fog is occurred three times more than the East Sea (Kim, 1988). The annual average days of sea fog occurrence in the central Yellow Sea and the south Yellow Sea is 60 and 78 days respectively (Kim, 1988). Fig. 1 shows the statistics of sea fog occurrence in year 2014. SC is Sokcho and UE is Ulleungdo in the East Sea. BY is Baengnyeongdo in the Yellow Sea, HS, WD and JD is Heuksando, Wando and Jindo weather stations in South Sea. Fig 1 shows that the highest occurrence is in the Baengnyeongdo, the island in the Yellow Sea.

Table 1 Specification of MODIS

<table>
<tr><td>Sensor</td><td colspan="8">Moderate-resolution Imaging Spectro-Radiometer (MODIS)</td></tr>
<tr><td>Orbit</td><td colspan="8">Polar</td></tr>
<tr><td>Coverage</td><td colspan="8">Entire globe</td></tr>
<tr><td>Altitude</td><td colspan="8">705 km</td></tr>
<tr><td>Radiometric resolution</td><td colspan="8">12 bit</td></tr>
<tr><td rowspan="19">Spectral Resolution [μm] / Spatial resolution [m]</td><td>R [m]</td><td>Band</td><td colspan="2">Wavelength</td><td>R [m]</td><td>Band</td><td colspan="2">Wavelength</td></tr>
<tr><td rowspan="2">250</td><td>Band 1</td><td>Red</td><td>0.65</td><td rowspan="18">1000</td><td>Band 19</td><td>NIR</td><td>0.94</td></tr>
<tr><td>Band 2</td><td>NIR</td><td>0.86</td><td>Band 20</td><td rowspan="6">SWIR</td><td>1.38</td></tr>
<tr><td rowspan="5">500</td><td>Band 3</td><td>Blue</td><td>0.47</td><td>Band 21</td><td>3.75</td></tr>
<tr><td>Band 4</td><td>Green</td><td>0.56</td><td>Band 22</td><td>3.96</td></tr>
<tr><td>Band 5</td><td>NIR</td><td>1.24</td><td>Band 23</td><td>3.96</td></tr>
<tr><td>Band 6</td><td>SWIR</td><td>1.64</td><td>Band 24</td><td>4.05</td></tr>
<tr><td>Band 7</td><td>SWIR</td><td>2.13</td><td>Band 25</td><td>4.47</td></tr>
<tr><td rowspan="11">1000</td><td>Band 8</td><td rowspan="3">Blue</td><td>0.41</td><td>Band 26</td><td>NIR</td><td>1.38</td></tr>
<tr><td>Band 9</td><td>0.44</td><td>Band 27</td><td rowspan="10">TIR</td><td>6.72</td></tr>
<tr><td>Band 10</td><td>0.49</td><td>Band 28</td><td>7.33</td></tr>
<tr><td>Band 11</td><td rowspan="2">Green</td><td>0.53</td><td>Band 29</td><td>8.55</td></tr>
<tr><td>Band 12</td><td>0.55</td><td>Band 30</td><td>9.73</td></tr>
<tr><td>Band 13</td><td rowspan="2">Red</td><td>0.67</td><td>Band 31</td><td>11.03</td></tr>
<tr><td>Band 14</td><td>0.68</td><td>Band 32</td><td>12.02</td></tr>
<tr><td>Band 15</td><td rowspan="4">NIR</td><td>0.75</td><td>Band 33</td><td>13.34</td></tr>
<tr><td>Band 16</td><td>0.87</td><td>Band 34</td><td>13.64</td></tr>
<tr><td>Band 17</td><td>0.91</td><td>Band 35</td><td>13.94</td></tr>
<tr><td>Band 18</td><td>0.94</td><td>Band 36</td><td>14.24</td></tr>
</table>

Table 2. Specifications of Terra and Aqua satellite

Satellite	Launched	Passing time (UTC)
Terra	1999.12.18	01:30-2:30 13:30-14:30
Aqua	2002.03.04	04:30-05:30 16:30-17:30

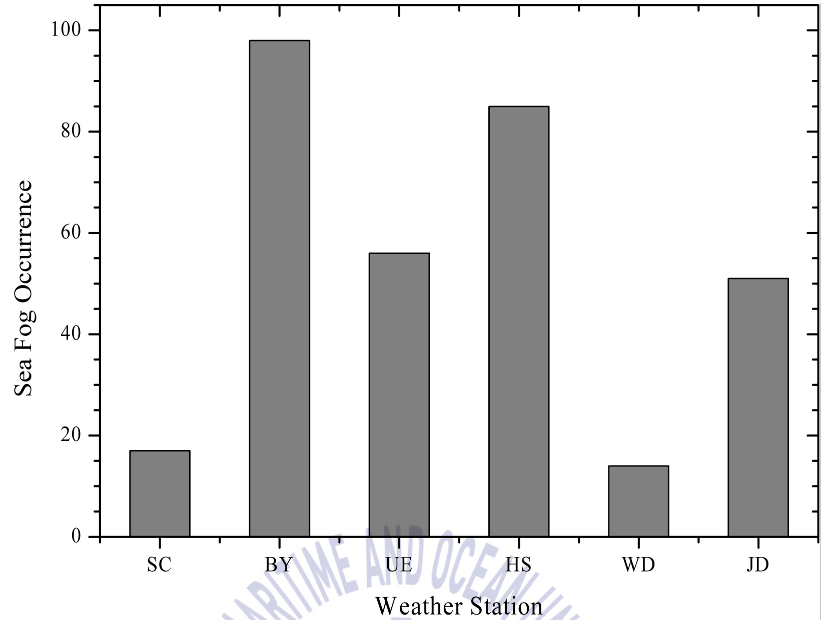

Fig 1. Statistics of sea fog occurrence around Korean Peninsula

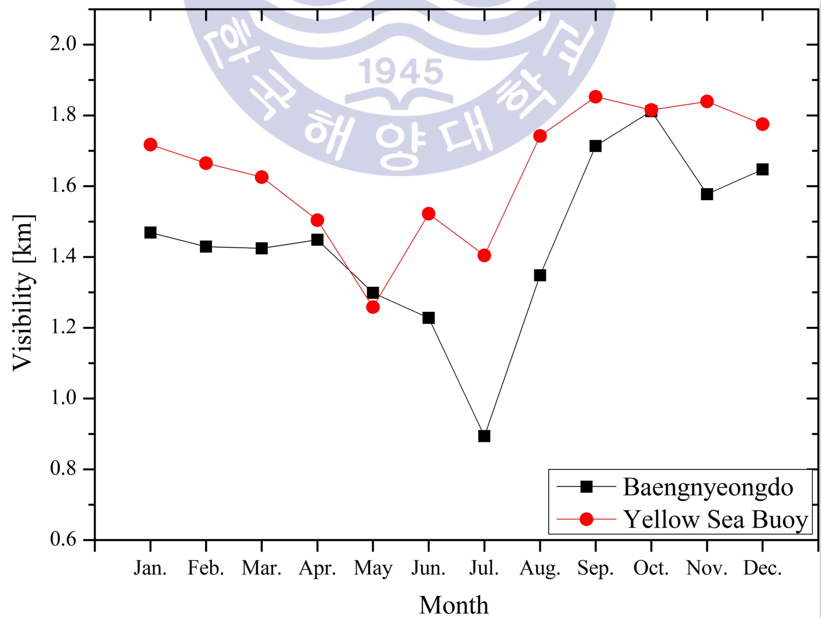

Fig. 2 Yellow Sea monthly average visibility observed from Baengnyeongdo and Yellow Sea buoy for 2013 to 2015

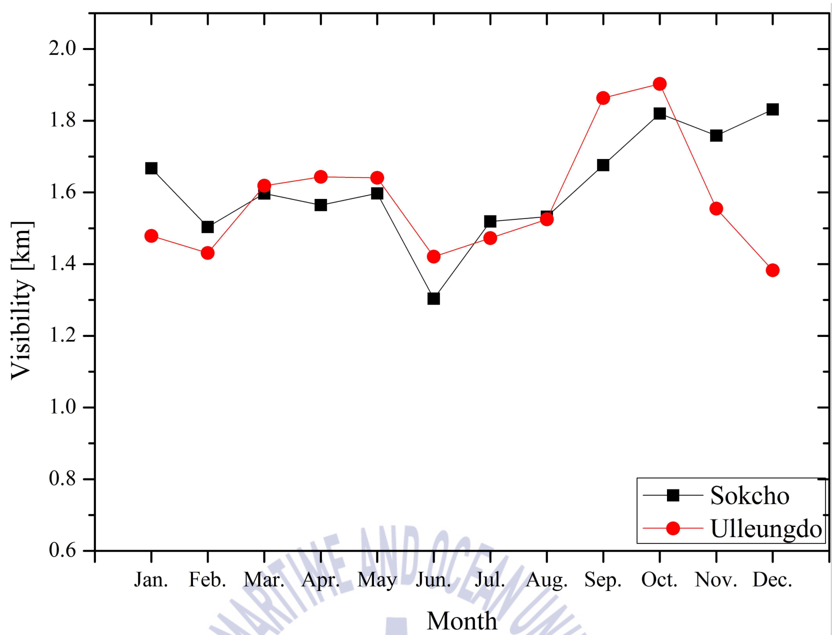

Fig. 3 South Sea monthly average visibility observed from Heuksando and Wando for 2013 to 2015

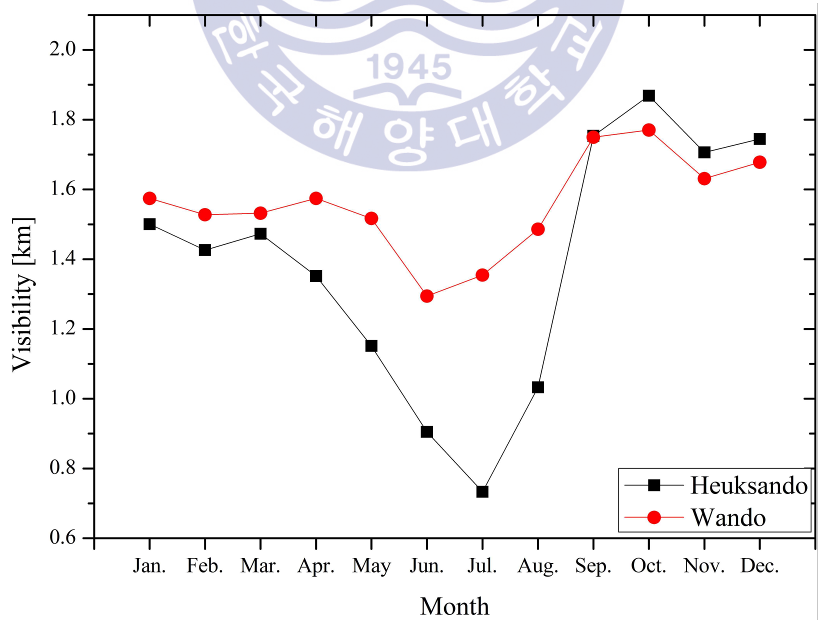

Fig. 4 East Sea monthly average visibility observed from Sokcho and Ulleungdo for 2013 to 2015

The weather station observation marked in Fig. 8 is showing where each weather station is located. The monthly average visibility of year 2013 to 2015 is displayed in Fig. 2 to Fig. 4 as for the Yellow Sea, the South Sea, and East Sea respectively. For the Yellow Sea, the Yellow Sea Buoy and Baeckroungdo is used as observation site and for the South Sea, the Heuksando and Wando observation site is used and for the East Sea, Sokcho and Ullengdo is used. The Yellow Sea and the South Sea indicate that the visibility is the low during spring and summer season. The East Sea shows relatively higher visibility compare to other seas. The higher visibility indicates that there are no sea fog occurred and so the region is more clear compare to lower visibility regions. The Yellow Sea indicates here again that the occurrence of sea fog is higher than the other sea.

1.2 Purpose and scope

The recent presented automatic sea fog detection algorithm presented by Wu and Li (2014) has already been used in semi-operational mode and successfully detected sea fog for daytime and night time using different algorithm for each time. However the detection result using the method presented by Wu and Li (2014) was showing some failure in detection for some cases in spring season sea fog in the Yellow Sea. The reason is preassumed to be unsuitable threshold for some indexes and damaged detector of the satellite spectrometer, Aqua/MODIS channel 6.

The purpose for this study is to present more suitable threshold value for each index and successful detection using both Terra and Aqua/MODIS data. The scope of this research is spring season daytime in the Yellow Sea as preliminary study. Although summer season has the highest occurrence of sea fog, this study is based on the spring season because it is hard to discriminate summer season scenes which often accompany the nimbus and rain which makes difficult to do manual detection for validation purpose.

Fig. 5 shows the flow of the contents and scopes in this research. In the following section 2, background of sea fog detection using satellite data is explained. Then the data set used in this study is explained. The methodology is described in detail for the improved sea fog detection method with validation method and the threshold decision method in section 4. The results and discussions are presented in section 5 followed by it and the conclusion is set at the last.

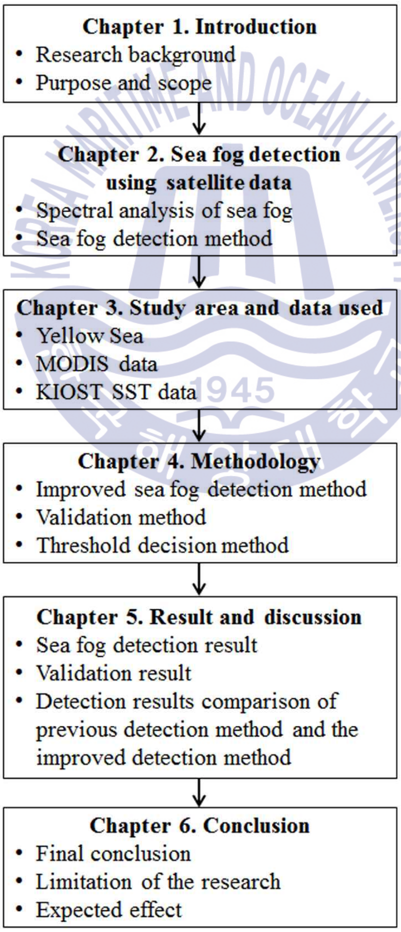

Fig. 5 Contents and scope of research

Chapter 2. Methods of detecting sea fog using visible and infrared channels

2.1 Sea fog characteristics

2.1.1 Visual characteristics of sea fog

Using color composit images, sea fog can be distinguished due to its surface homogeneity. For true color composite image, it is known to use combination of band 1 (0.65 μm), 4 (0.56 μm) and 3 (0.47μm). In true color composite image, clouds look bright white and sea fog often looks similar but slightly less bright than the mid/high clouds. Using false color composite of band 5 (1.24 μm), 2 (0.86 μm), 1 (0.65 μm), the mid/high clouds are displayed in cyan color, the stratus are in white color and the sea fog is in bright grey color (Fig. 6). Sea fog and stratus are distinguisable using the smoothness of the surface. Each region of sea fog, low stratus and mid/high cloud are in 40 km x 40 km (1600 pixels) for spectral analysis (Fig. 6).

2.1.2 Optical characteristics of sea fog

To detect sea fog, we had to analyse the spectral characteristics of sea fog and other clouds. Hao et al., (2009) have already presented the result of the spectral characteristics of sea fog and other properties of MODIS band 1 to 7 with spectral range of 0.4 μm to 2.2 μm (see Fig. 6). Clouds are having higher reflectance but lower brightness temperature than sea fog. Using this spectral characteristic, many cloud detection method were developed (Ackerman et al., 1998; Stowe et al., 1999; Kriebel et al., 2003; Wang and Shi, 2006).

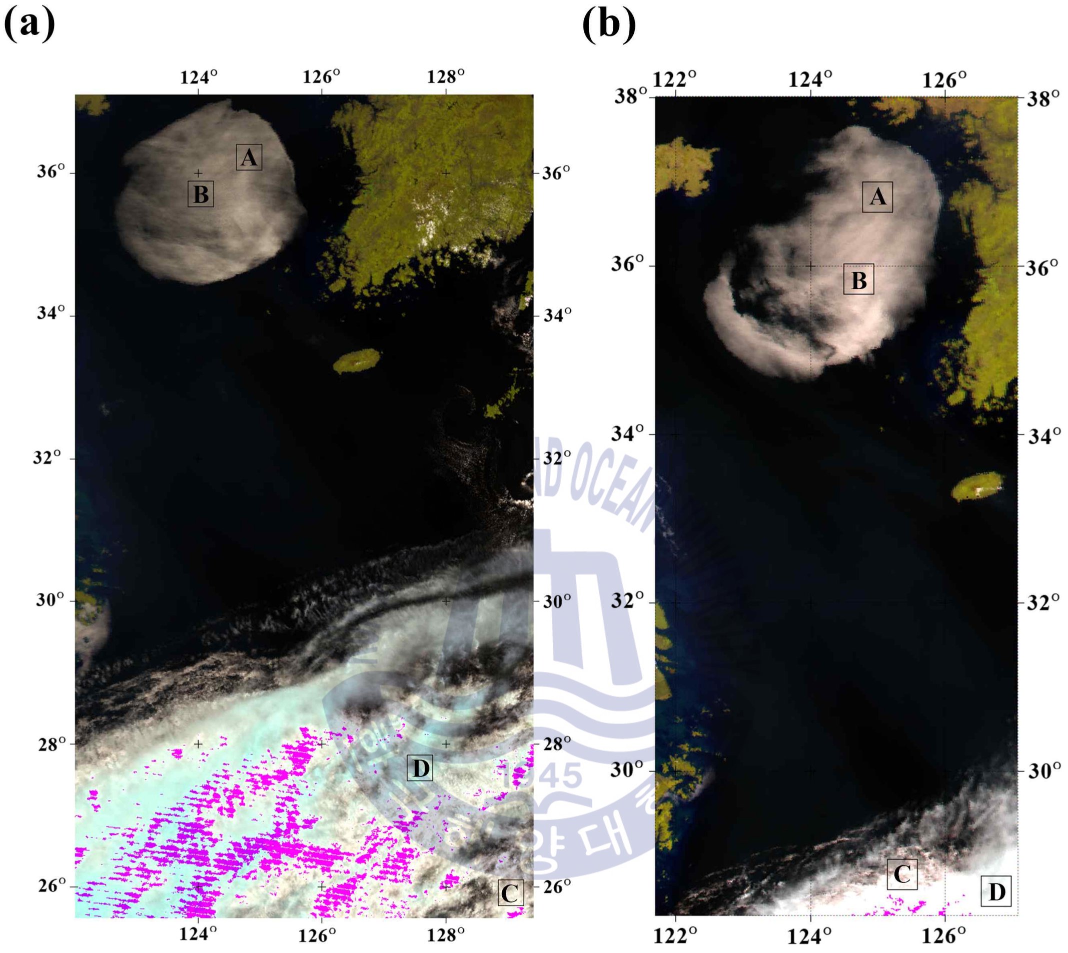

Fig. 6 False color composite image of band 5, 2 and 1 for 2014 May 1 of (a) 02:10 (UTC) and (b) 05:25 (UTC). The selected regions of A: sea fog 1, B: sea fog 2, C: Mid/High clouds, D: Low stratus is shown above (Each region is 40 km x 40 km with 1600 pixels).

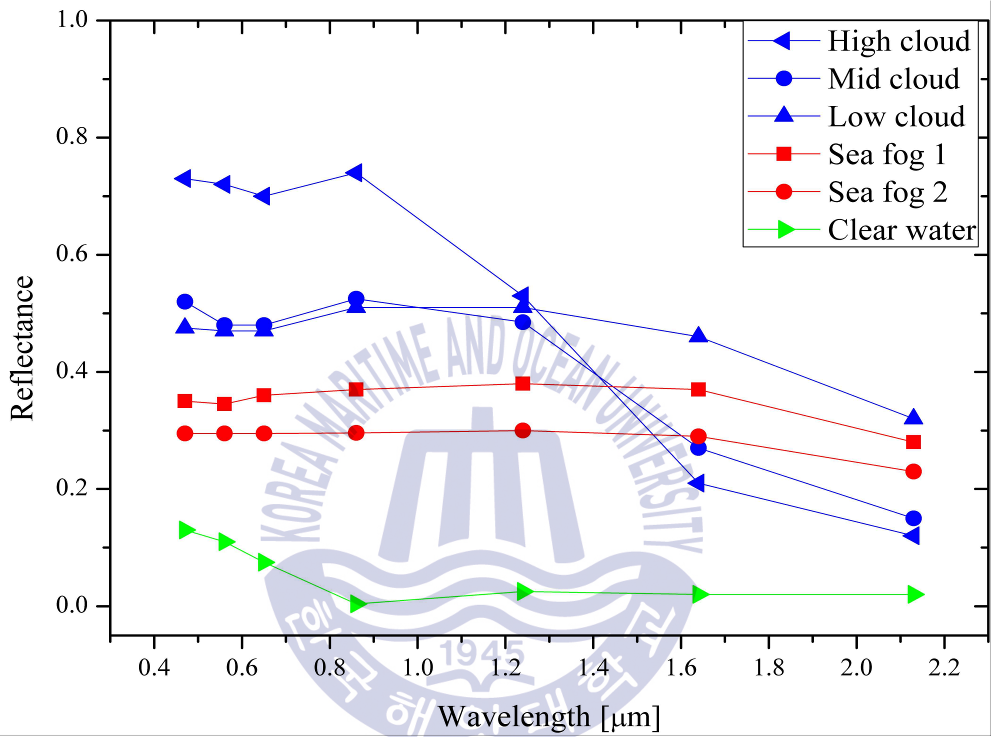

Fig. 7 Reflectance of MODIS band 1 – 7 at different sea fog and other regions (adapted from Hao et al., 2009)

The analyzed results indicate that the reflectance of low stratus and mid/high clouds are higher than sea fog in range of visible to near infrared band (Fig. 8). The reflectance of low stratus is showing little higher than sea fog but in overall, they have similar pattern due to their microphysical similarities. Therefore it is hard to distinguish them in visible reflectance. However, mid/high clouds are showing relatively low reflectance in short wavelength infrared (SWIR) compare to the reflectance in visible and near infrared (NIR) wavelength. The purple region is error caused by no value in band 2 (0.87 μm, NIR).

Fig. 9 shows the spectral analysis of water vapor channels of Band 17 - 19 (0.90 - 0.94 μm). It shows that sea fog has lower reflectance compare to low stratus and mid/high clouds. Band 17 (0.90 μm) is showing the highest reflectance which means it is most sensitive to water vapor and is least sensitive in band 18 (0.94 μm). These spectral characteristics can be used to discriminate sea fog and other clouds using the most sensitive channel and the least sensitive channels.

The emissivity from the thermal infrared channel is converted to the brightness temperature. Fig. 10 is showing the wavelength of 3.7 to 14.3 μm which is analyzed for sea fog, low stratus and mid/high clouds. It shows that the band 31 (11 μm) has relatively big difference for sea fog and other clouds compare to other spectral band. For example, the standard deviation of sea fog in band 31 is less than 0.2 when other clouds are above 3. Whereas band 22 of 3.9 μm has sea fog standard deviation of less than 3 which is similar to mid/high cloud standard deviation values.

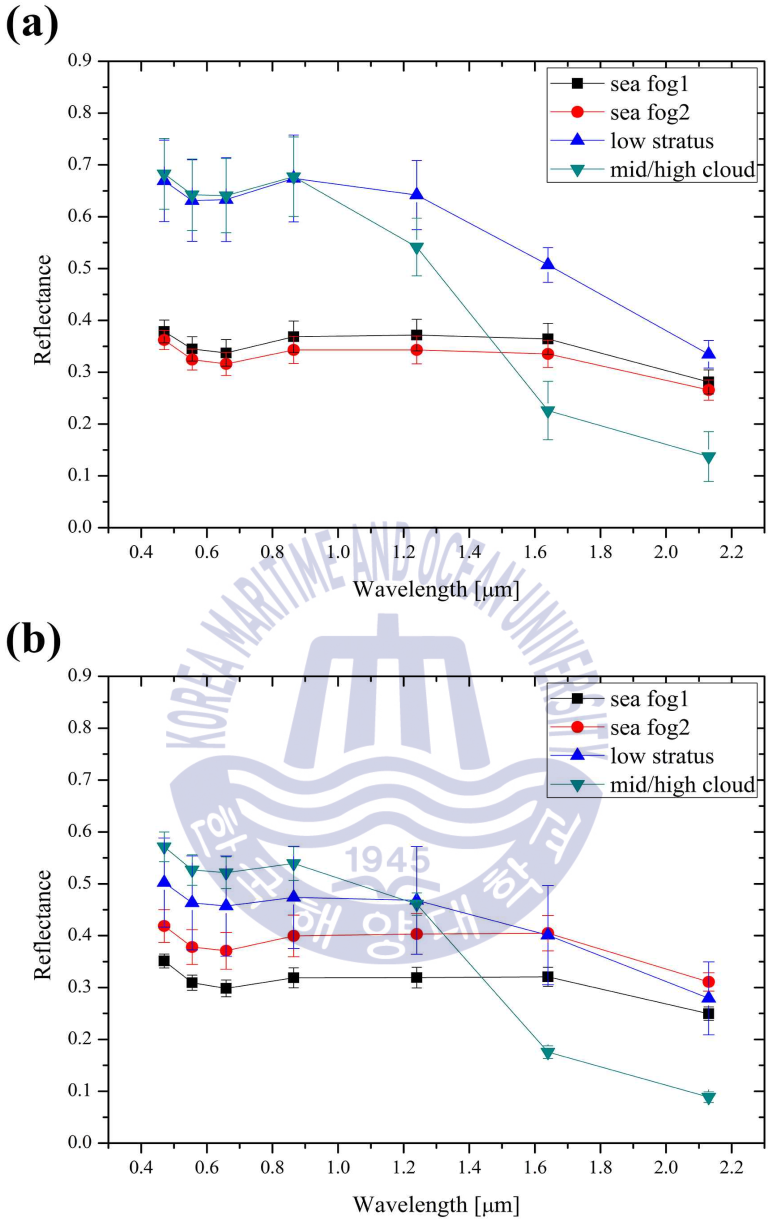

Fig. 8 Reflectance of the spectral bands from 0.4 to 2.2 μm is presented. Each line indicate sea fog 1, sea fog 2, low stratus and mid/high clouds which are extracted from the selected regions indicated in Fig. 4. for 2014 May 1 of (a) 02:10 (UTC) and (b) 05:25 (UTC)

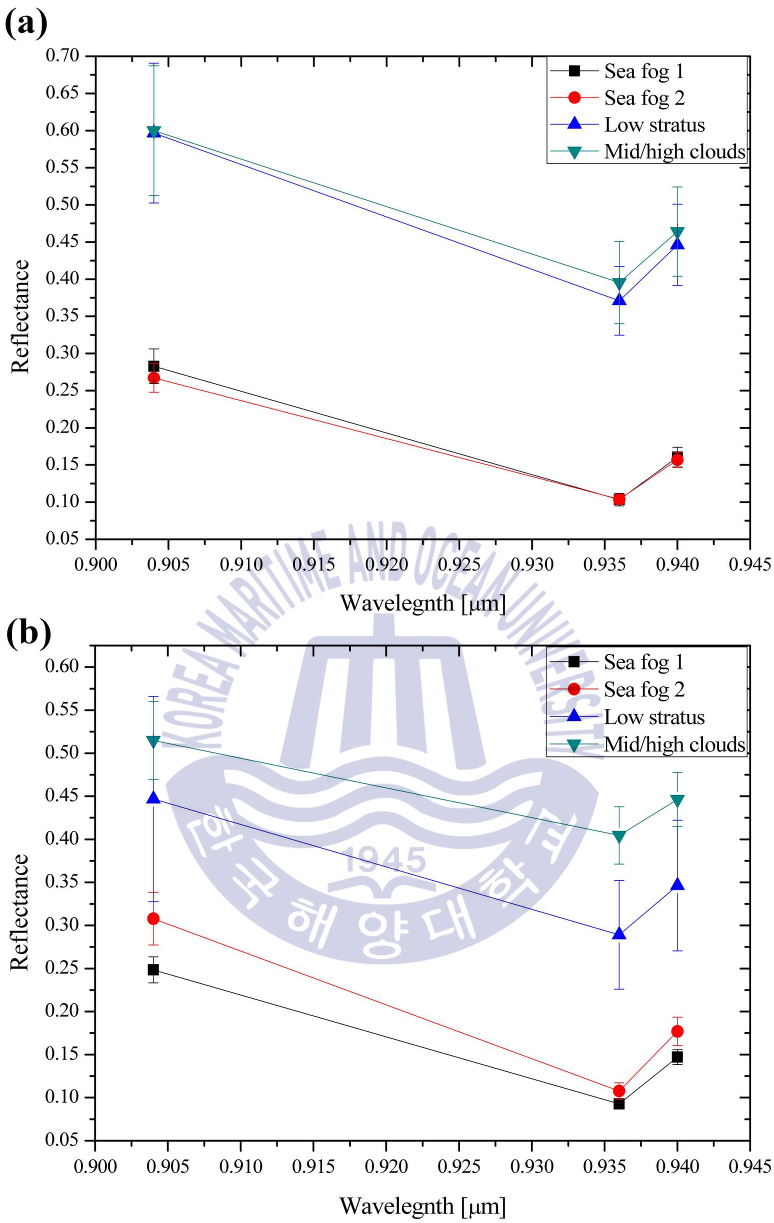

Fig. 9 Reflectance of the water vapor bands (band 17: 0.90 μm, band 18 0.93 μm, band 19: 0.94 μm) is presented. Each line indicate sea fog 1, sea fog 2, low stratus and mid/high clouds which are extracted from the selected regions indicated in Fig. 4. for 2014 May 1 of (a) 02:10 (UTC) and (b) 05:25 (UTC)

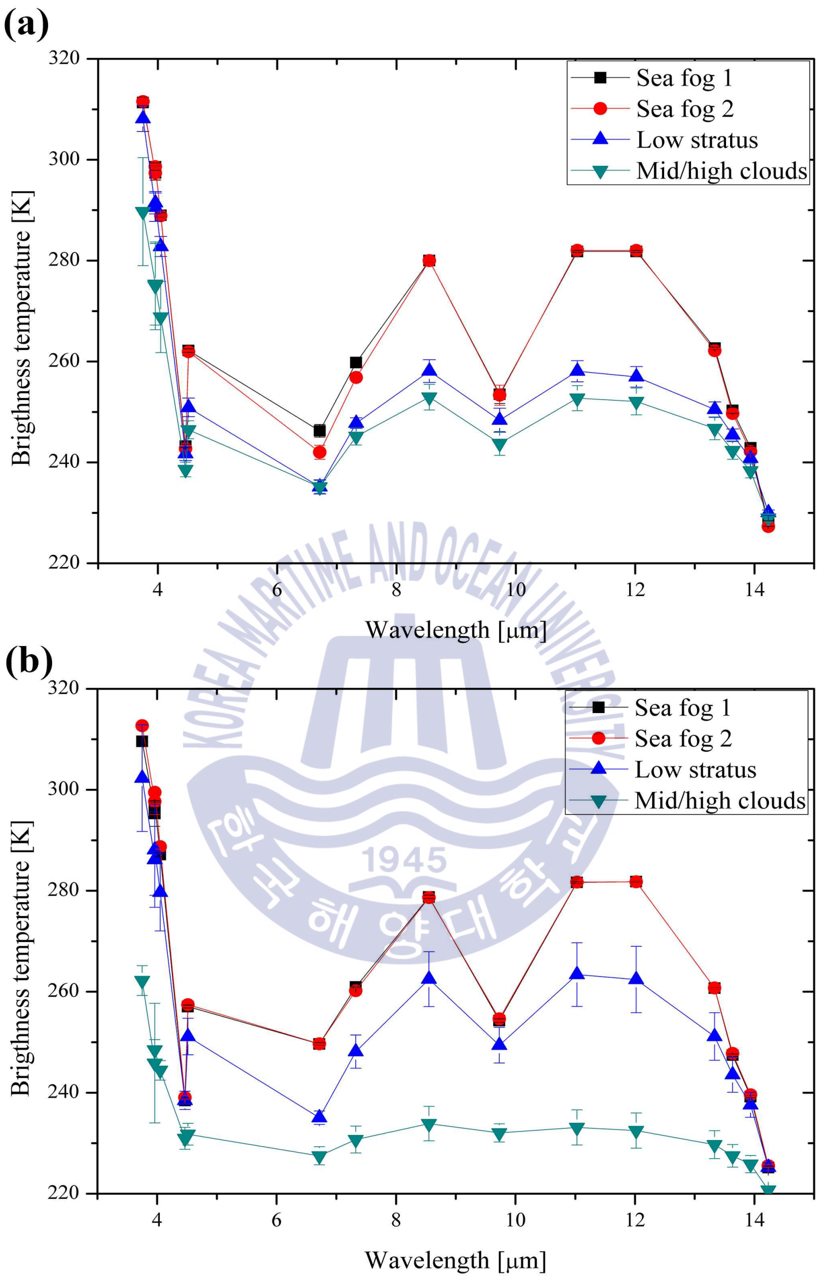

Fig. 10 Brightness temperature of the spectral bands from 3.6 to 14.3 μm is presented. Each line indicate sea fog 1, sea fog 2, low stratus and mid/high clouds which are extracted from the selected regions indicated in Fig. 4. for 2014 May 1 of (a) 02:10 (UTC) and (b) 05:25 (UTC)

2.2 Sea fog detection method

2.2.1 Manual detection method

Using color composite image, sea fog that occurs during daytime can be detected manually due to its characteristics of reflectance and smooth surface (Ahn et al., 2008, Gao et al., 2009). In this study, manual detection involves using image analysis software such as ENVI. With the color composite image, sea fog is distinguished through visual inspection. After manual detection using ENVI region of interest (ROI) tool in polygon, it requires to distinguish sea water and sea fog. To discriminate sea water, the simple threshold of near infrared band can be used. It is because the sea water have almost zero reflectance in near-infrared. The manual detection result is shown in Fig. 11.

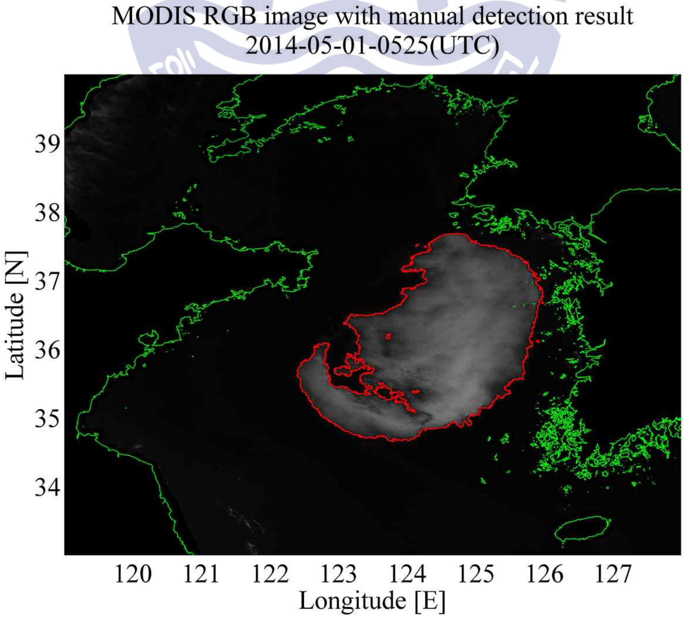

Fig. 11 The manual detection result in red closed line on the RGB composite image

2.2.2 Dual channel difference

In many studies, sea fog/low stratus was detected using dual channel difference (DCD) method because it is easier to discriminate fog/low stratus from other objects using the difference of the brightness temperature at 3.9 μm channel and 11 μm. Due to the reduced emissivity of clouds with small droplets in the 3.7 μm, the sea fog has less difference between two channel compare to mid/high clouds (Hunts 1973; Eyre et al., 1984; Bendix and Bachmann 1991; Ellord 1995; Turner et al., 1986; Ann et al., 2003; Bendix et al., 2004). However DCD method was only used for night-time because in the daytime, the small fog droplets reflect at 3.7 μm wavelength which leads to the contamination of the solar radiation and requires some other approach to detect daytime sea fog (Cermak and Bendix, 2008). Another problem of DCD method is that there are limits on discriminating sea fog and low stratus since they share similar spectral features.

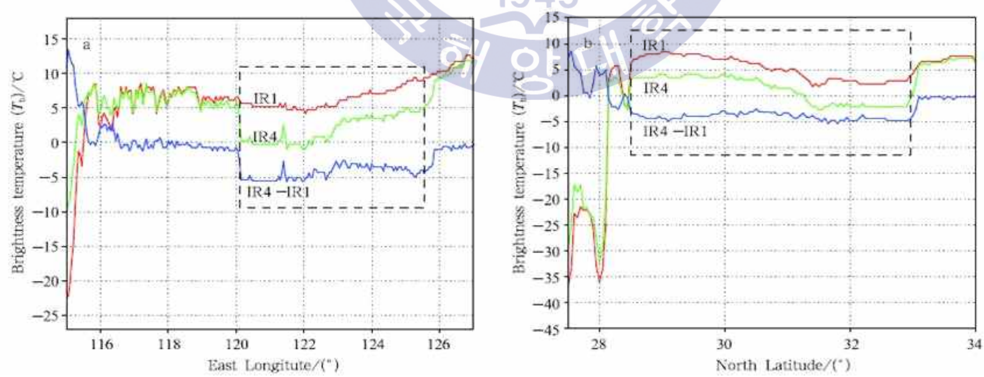

Fig. 12 Brightness temperature of IR1, IR4 and IR4 - IR1 data of MTSAT-1R. The dashed frame indicates the sea fog/stratus are (adapted from Gao et al., 2009)

2.2.3 Texture analysis

Unlike other clouds, sea fog has very homogeneous surface texture. Mainly it is because sea fog is formed when the atmosphere is in stable condition. Using this characteristic, sea fog is detected through texture analysis. Sea fog emissivity in thermal infrared shows less variations when other clouds emissivity shows more variations in the thermal band.

Heo et al. (2008) discriminates sea fog and low stratus using the homogeneity characteristics of sea fog compare to low stratus. They also used MODIS Cloud Top Pressure (CTP) data as the reference of sea fog and low stratus cases. When CTP is above 680 hPa, it was assumed to be sea fog or low stratus case. Among them, when sea fog is observed in ground observation station, it was determined as sea fog case. They calculated standard deviation value after detecting sea fog and low stratus using dual channel difference method.

Like as, the texture analysis method is possible to be adapted to many kinds of satellite data where IR channel is present such as AVHRR, MTSAT, MODIS, GOES, etc. However single texture analysis is not enough to distinguish all stratus from sea fog regions.

Fig. 13 is showing that (a) and (b) is showing almost no variation compare to (c) and d) in 11 μm channel. More variation indicates that the surface is not smooth which means that it is not a sea fog case.

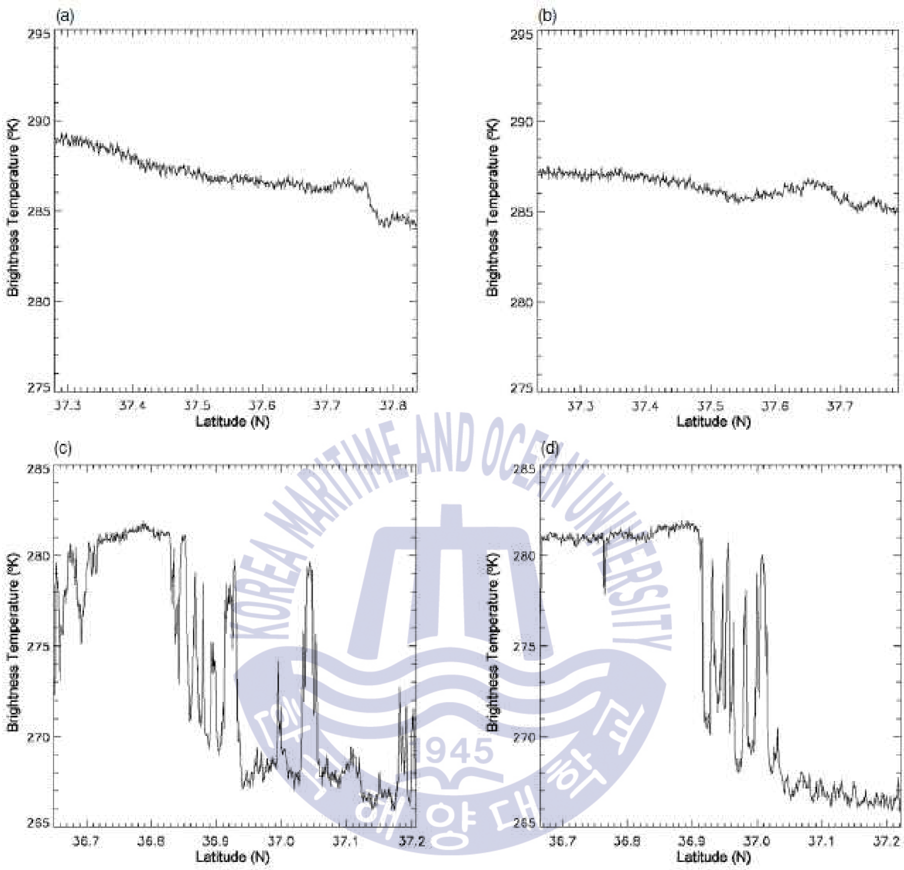

Fig. 13 Spatial profile of 11.3 mm brightness temperature measured by ATSTER satellite for sea fog in (a) and (b) and stratus in (c) and (d) (Adapted from Heo et al.,2008)

2.2.4 Threshold scheme

Another method used mainly is threshold scheme. It is known as an effective method to detect for both daytime and nighttime sea fog with different flow chart. It is proceed with various indexes in order according to the characteristics of sea fog. However, the procedure is relatively complex compare to other single index process. Many sea fog detection method used threshold scheme (Zhang and Yi, 2013; Wu and Li, 2014). Zhang and Yi (2013) suggested a comprehensive dynamic threshold algorithm to detect daytime sea fog MODIS. The vertical structures of fog and stratus were analyzed using in-situ data of ground sounding station. They derived monthly dependent threshold for TAT- SST (TAT: temperature at tops of fog or stratus, SST: sea surface temperature).

For automatic detection of sea fog using Terra/MODIS data, Wu and Li (2014) used algorithms for daytime and night-time using dual channel difference, the normalized difference snow index (NDSI), the brightness temperature difference of cloud and clear sky sea surface (BTD_{back}), the normalized difference near-infrared water vapor index (NWVI), and the NWVI difference between a possible fog/stratus cloud pixel and a nearby clear-sky ocean pixel (D_NWVI) based on a threshold scheme. However the algorithm result showed some failure in detecting, when using Aqua/MODIS data and also showing some miss in detection. The comparison will be presented in section 5, result and discussion. The flow chart of the algorithm is presented in Fig. 14.

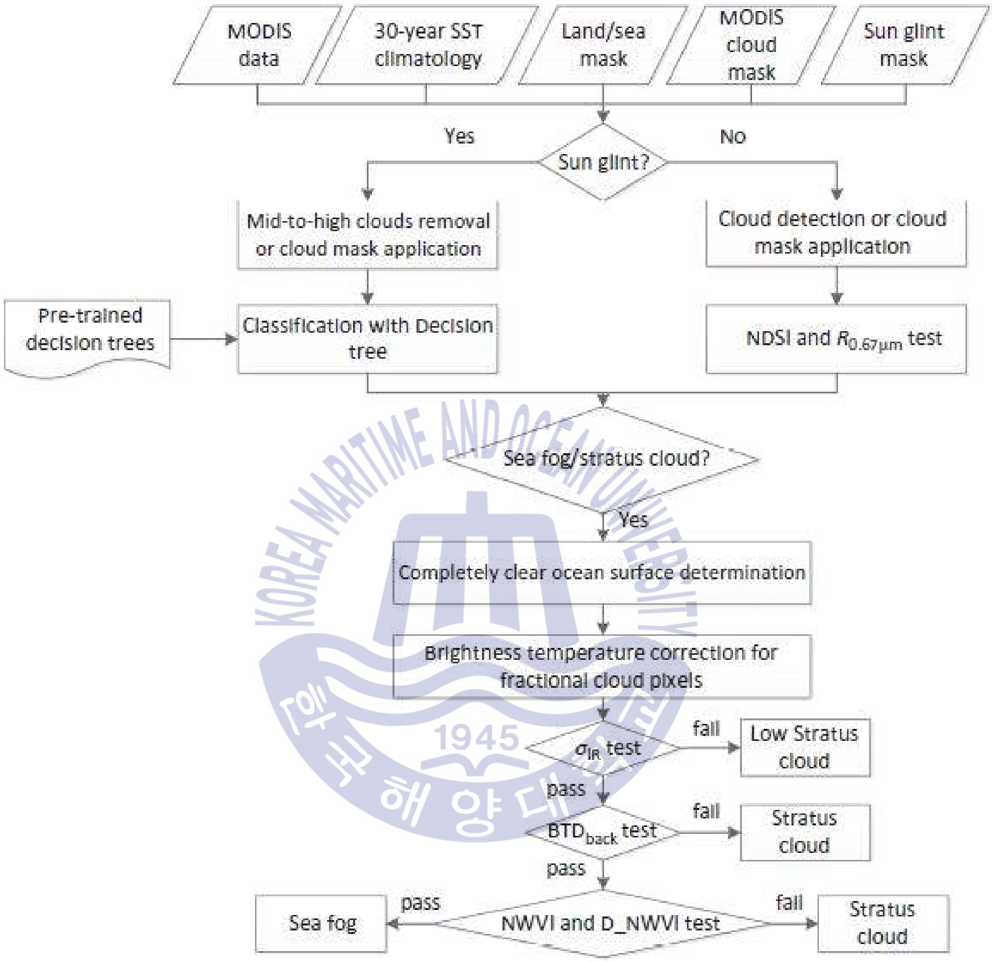

Fig. 14 Algorithm flow chart for automatic sea fog detection in daytime presented in Wu and L., 2014 (adapted from Wu and Li, 2014)

2.3 Summary

Sea fog detection using satellite data has gone through a lot of development. However, among many detection methods, none of the method is perfect and therefore combinations of several indexes which are derived from the spectral characteristics of sea fog and other cloud is required. Dual channel difference index is only adaptable to night time detection, due to the effect on solar radiance in 3.9 μm. Also, with the microphysical similarity of low stratus and sea fog, it is difficult to distinguish, so it requires other process to remove low stratus. Texture analysis is possible to adapt many kinds of satellite data where IR channel is present. It is adaptable to both daytime and night time and effective to remove low stratus clouds after removal of mid/high clouds. However, texture analysis of single detection method is not enough to distinguish all stratus and requires some other process to remove remaining clouds. The recent automatic sea fog detection method presented by Wu and Li (2014) also used various indexes and adapted threshold for winter season and non-winter season with two different algorithm for daytime and night time detection algorithms. This kind of threshold scheme is yet the most effective method which includes various indexes according to the characteristics of sea fog. However, it requires complex procedure and requires wide range of spectrum data.

Chapter 3. Study area and dataset used

2.1 Yellow Sea

This study used MODIS data to detect sea fog occurred in the Yellow Sea which has the highest occurrence among the coast near Korean Peninsula. We focused on the sea fog cases in spring season because it occurs mostly on spring and summer. However there were MODIS is loaded on Terra and Aqua spacecraft which are polar-orbiting satellites and observe the Yellow Sea twice a day therefore total of four data is obtained every day. The study area is the Yellow Sea near the Korean Peninsula (Fig. 15).

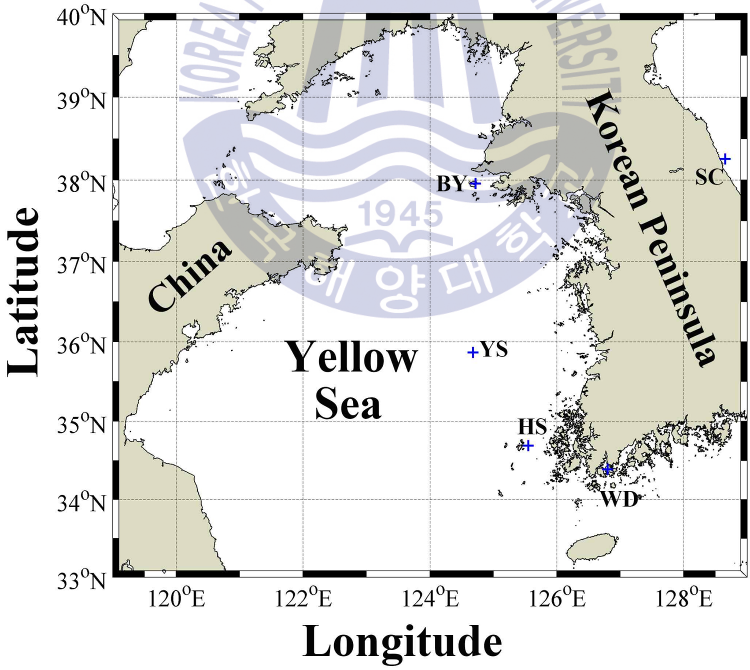

Fig. 15 Map of study area showing the Yellow Sea near Korean coast of 778 km x 838 km (119 – 128° E, 33 – 40° N). Each cross mark indicate the location of weather stations as BY: Baeckroungdo, YS: Yellow Sea Buoy, HS: Heuksando, WD: Wando, SC: Sokcho.

3.1.1 Geomorphological characteristics

The Yellow Sea is located between the main land of China and Korean Peninsula and it is a marginal sea of Pacific Ocean. The maximum depths is less than 100 m because it is a continental shelf sea where as the mean depths of the East Sea is over 1000 m (Cho et al., 2000). The maximum velocity of the tidal current in the Yellow Sea is 1.5 m/s (Lee 1992). This kind of shallow water depth and fast tidal current makes affordable condition to form sea fog.

3.1.2 Meterological characteristics.

The Yellow Sea has a warm cyclone current and it is part of the Kuroshio Current which is diverges near the western part of Japan and flows northward into the Yellow Sea with speed below 0.8 km/h. The Tsushima Current originated from Kuroshio, heats up East Sea South Sea however Yellow Sea is not getting as must as heat. This induce the difference in sea surface temperature and the air temperature which makes more affordable condition for sea fog to be formed.

3.2 Weather station observation *in-situ* data

The average sea surface air pressure relative humidity measured from Baeckroungdo weather observation station from 2000 to 2015 is presented in Fig. 16. The air pressure of sea surface is the lowest in July whereas the occurrence of the sea fog is the highest (Fig. 16(a)). Yellow Sea have very wet summer as shown in Fig. 16(b) From the weather observation in situ data shows that sea fog occurrence when the air pressure of sea surface is low and high humidity.

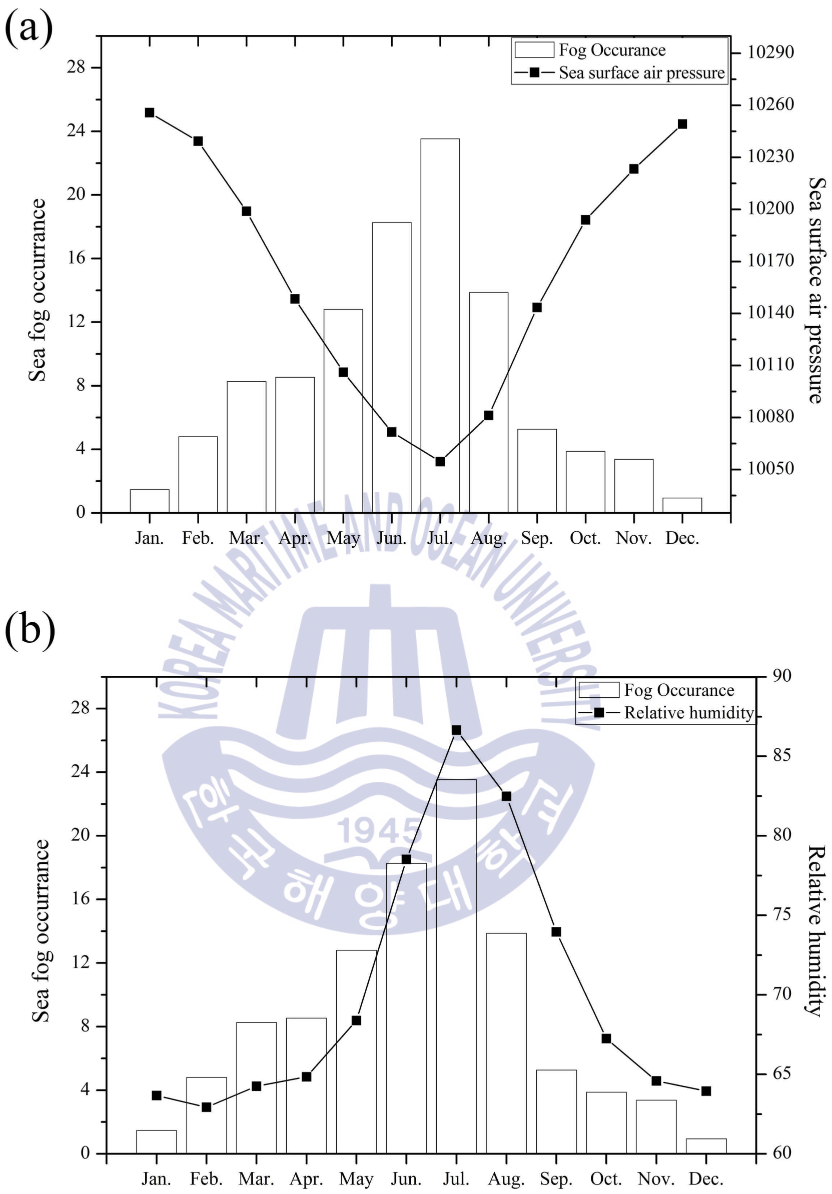

Fig. 16 Monthly averaged air pressure of sea surface in (a) and monthly averaged relative humidity observed in BY weather station from 2000 to 2015 with average sea fog occurrence in bar graph

3.3 Moderated-resolution Imaging SpectroRadiometer (MODIS)

In this study, we used MODIS data downloaded from LAADS Website (Level 1 and Atmosphere Archive and Distribution System, https://ladsweb.nascom.nasa.gov). MODIS have wide spectral range of visible (VIS) to thermal infrared (TIR) with 36 spectral channels composed of 20 reflective and 16 emissive channels. This provides more opportunities to improve sea fog monitoring and detection method (Bendix et al., 2005). The list of the MODIS data MODIS Level 1B calibrated radiance at 1 km resolution (MOD /MYD021KM), MODIS geolocation data (MOD/MYD03) and MODIS Level 2 cloud mask product at 1km resolution (MOD/MYD35) which was downloaded from LAADS Website (Level 1 and Atmosphere Archive and Distribution System, https://ladsweb.nascom.nasa.gov).

To convert the data into reflectance and brightness temperature, we used the MODIS Conversion Toolkit (MCTK, version 2.0.2) which is a plugin of ENVI software (Devin, 2014), With MODIS geolocation data, it applied the map projection of Geographic Latitude/Longitude. The data is then masked land area using MOD/MYD03 Land/Sea Mask product.

The MODIS L1B data is in scaled integer (SI) scientific data sets (SDS) with calibrated MODIS Earth view data. The calibrated data is converted to top-of-atmosphere (TOA) reflectance. The equation to convert TOA reflectance is described as equation (1).

TOA reflectance =

$$reflectance\_scales_B \ (Scaled\ integer - reflectance\_offsets_B) \quad (1)$$

The emissivity of the thermal infrared band is converted to the brightness temperature with units of Kelvin degree Celsius by the inversion of Planck's equation shown in equation (2).

$$T = \frac{c_2 v}{In(1 + (\frac{e c_1 v^3}{E}))} \quad (2)$$

where c_1 is 1.1910659 x 10^{-5} mW m^{-2} sr cm^{-4}, c_2 is 1.438833 cm degree Kelvin, v is central wavelength in cm^{-1}, E is the radiance from MODIS in mWm^{-2} sr cm^{-4} and e is emissivity.

3.3.1 MODIS Level 1B calibrated radiance at 1 km resolution (MOD/MYD21KM)

The MODIS Level 1B radiance data is produce from NASA MODIS atmosphere team and provided in the website. It contains Calibrated Earth View data at 1km resolution, including the 250 m and 500 m resolution bands aggregated to 1km resolution.It is in Hierarchical Data Format (HDF) which is the standard data sotrage format selected by the Earth Observing System Data and Information System (EOSDIS) Core System (ECS).

3.3.2 MODIS geolocation data (MOD/MYD03)

The MODIS geolocation data contain geodetic latitude and longitude, surface\height above geoid, solar zenith and azimuth angles, satellite zenith and azimuth angles, and a land/sea mask for each 1 km sample. This data has been used for making land mask of each scene and map projection of Geographical Longitude/Latitude.

3.3.3 MODIS cloud mask data (MOD/MYD35_L2)

The MODIS cloud mask data contains some of the subsets form MODIS geolocation product (MOD/MYD03) such as scan start time, solar zenith/azimuth angle, sensor zenith/azimuth angle. The Cloud Mask scientific data set (SDS) contains 48 bit MODIS cloud mask product. Each bit in the MODIS cloud mask product contains the information on surface. Each bits are the results of tests such as the Infrared brightness temperature threshold and difference (BTD) test, the visible and near- infrared threshold tests, the additional clear sky restoral tests and etc.

Table 3. List of training data

Case number	Platform	Data and time (UTC)
Case 1	Terra	2014.03.16. 01:55
Case 2	Terra	2014.03.23. 02:00
Case 3	Aqua	2014.03.23. 05:20
Case 4	Aqua	2014.04.08. 05:20
Case 5	Terra	2014.04.24. 01:55
Case 6	Terra	2014.05.01. 02:10
Case 7	Aqua	2014.05.01. 05:25
Case 8	Terra	2016.03.30. 01:50
Case 9	Aqua	2016.03.30. 05:05

Table 4. List of test data

Case number	Platform	Data and time (UTC)
Case 1	Terra	2013.03.04. 02:00
Case 2	Aqua	2013.03.04. 05:20
Case 3	Aqua	2013.03.07. 04:10
Case 4	Terra	2013.03.08. 03:15
Case 5	Aqua	2013.03.08. 04:55
Case 6	Terra	2013.04.04. 02:55
Case 7	Terra	2013.05.04. 03:10
Case 8	Aqua	2013.05.04. 04:50
Case 9	Terra	2013.05.05. 02:15
Case 10	Aqua	2013.05.11. 04:55
Case 11	Aqua	2013.05.21. 05:30
Case 12	Terra	2015.03.22. 02:25
Case 13	Aqua	2015.03.22. 04:05
Case 14	Terra	2015.03.26. 02:00
Case 15	Aqua	2015.03.26. 05:20
Case 16	Terra	2015.05.14. 02:45
Case 17	Aqua	2015.05.14. 04:25
Case 18	Aqua	2015.05.24. 05:00
Case 19	Terra	2015.05.26. 03:10

3.4 Geostationary Ocean Color Imagery (GOCI)

COMS (Communication, Ocean, and Meteorological Satellite), the first Korean geostationary meteorological satellite was launched on 27 June 2010. The Geostationary Ocean Color Imagery (GOCI) is the world's first ocean observation geostationary satellite which is loaded on COMS. It observes the study area eight times per day for 30 minutes observation and rest for 30 minutes from 09:15 to 16:15 (KST). GOCI has six visible bands and two near-infrared bands. The GOCI L1B data are downloaded from Korea Ocean Satellite website (http://kosc.kiost.ac/kosc_web/GOCI_download/SatelliteData.html). The true color composite of GOCI is used as reference of sea fog cases. The GOCI data is used for the similar time that matches with the list of data on Table 3 and 4. Fig. 17 shows GOCI flase color composite image with no land masking.

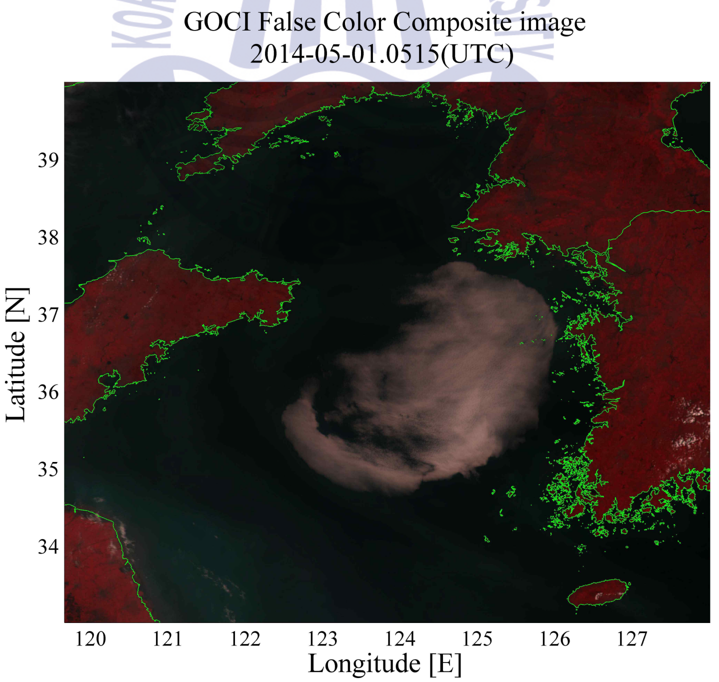

Fig. 17 GOCI false color composite image of 2014-05-01. 05:15 (UTC) with sea fog occurred in the Yellow Sea

3.5 Meteorological Imagery (MI)

The fog product produced using Meteorological Imagery (MI) is observed every 15 minutes with 4 km spatial resolution. The MI/Fog product is used as reference to verify if the case is actual sea fog or not.

Table 5 Details of MI and GOCI channels

	Channel	Wavelength (μm)	Spatial Resolution (km)
MI	Visible	0.675	1 x 1
	SWIR	3.75	4 x 4
	Water Vapor	6.75	4 x 4
	IR	10.8	4 x 4
	IR	12	4 x 4
GOCI	Band 1 - Blue	0.412	1 x 1
	Band 2 - Blue	0.443	1 x 1
	Band 3 - Blue	0.49	1 x 1
	Band 4 - Green	0.555	1 x 1
	Band 5 - Red	0.66	1 x 1
	Band 6 - Red	0.68	1 x 1
	Band 7 - NIR	0.745	1 x 1
	Band 8 - NIR	0.865	1 x 1

3.6 KIOST Sea Surface Temperature

The sea surface temperature is used to discriminate sea fog and stratus using the temperature difference between the brightness temperature of cloud top and the sea surface temperature. We used a high resolution sea surface temperature (SST) product generated daily by Korea Institute of Ocean Science and Technology (KIOST). The SST product is comprised of four sets of data including eight-hour and daily average SST data of 1 km resolution, and is based on the four infrared (IR) satellite SST data acquired by advanced very high resolution radiometer (AVHRR), Moderate Resolution Imaging Spectroradiometer (MODIS), Multifunctional Transport Satellites-2 (MTSAT-2) Imager and Meteorological Imager (MI), two microwave radiometer SSTs acquired by Advanced Microwave Scanning Radiometer 2 (AMSR2), and WindSAT with *in-situ* temperature data. The input data are merged by using the Optimal Interpolation (OI) algorithm (Yang et al., 2015). The KIOST SST product is downloaded from FTP server. The coverage of the product is longitude of 117.25° - 133.73° E and latitude of 32.51° - 41.48° N which is centered at the Korean Peninsula. The daytime SST product of (23 - 16) is used for the date of the data used for detecting sea fog mentioned on Table 3 and Table 4.

Chapter 4. Methodology

4.1 Improved sea fog detection method

Based on the spectral and physical features of sea fog, the improved algorithm using MODIS data is presented in Fig. 18. To detect daytime sea fog, first extract cloudy area which includes sea fog and other clouds using MODIS Cloud Mask Product. Then through following steps, we distinguish other clouds and excluded those pixels. The threshold was optimized for the Yellow Sea near Korean coast in spring season. The algorithm includes using MODIS cloud mask product, Normalized Water Vapor Index (NWVI), standard deviation test of 11 μm infrared band, Normalized Difference Snow Index (NDSI) and the Temperature Difference Index (TDI).

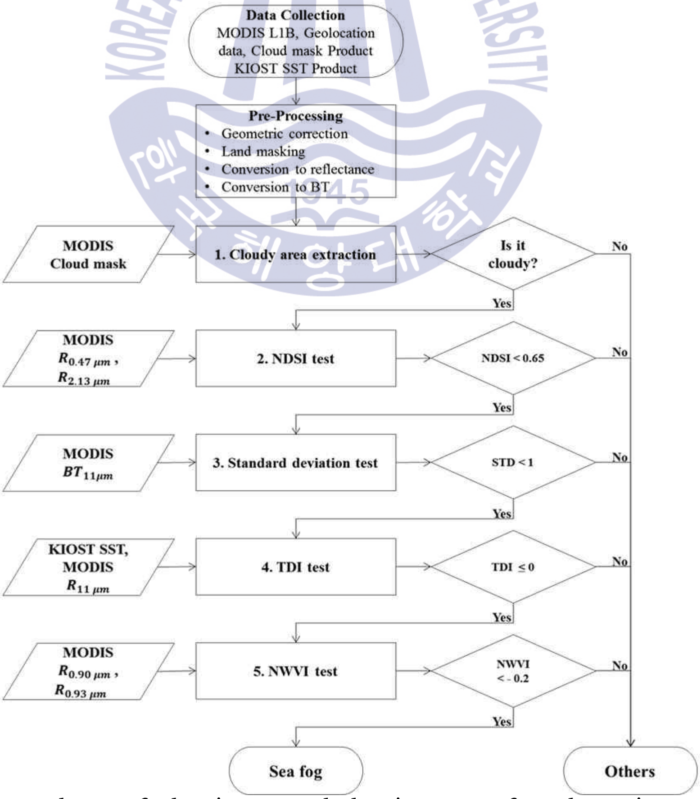

Fig. 18 Flow chart of the improved daytime sea fog detection algorithm

4.1.1 Cloud mask application

Using the MODIS Levle 2 cloud mask product in Hierarchical Data Format (HDF), we extract the actual cloud mask data which is contained in the 48 bits. In the bit field 1-2, the cloudy region can be retrieved. The final confidence flag for the field of view (FOV) was determined into four categories: confident clear, probably clear, probably cloud and confident cloud (see Table 6) through many individual tests (Ackerman et al. 2010). We defined probably cloud and confident cloud as cloudy pixels as we can detect cloudy area first. The cloudy area includes sea fog, other clouds such as mid/high clouds, low stratus and even some parts that are not clear and not cloud. With the detected region, other properties rather than sea fog will be eliminated along the following processes.

Table 6 The MODIS Cloud mask information of bit 1 - 2

Cloud State	Bit	Quality threshold
Confident cloudy	00	Confidence ≤ 0.66
Probably cloudy	01	0.95 ≥ confidence > 0.66
Probably clear	10	0.99 ≥ confidence > 0.95
Confident clear	11	confidence > 0.99

4.1.2 Normalized difference snow index (NDSI)

After extracting cloudy area, the detected region is used to calculate the normalized difference snow index (NDSI). The NDSI was originally developed to distinguish snow and non-snow pixels (Doizier 1989; Dozier and Painter 2004; Salomonsona and Appel 2004; Cermak and Bendix 2008). Middle/high clouds share similar features with snow because they are mixed clouds, so it includes ice and snow crystals components (Zhang 1992, Zhang and Yi 2013). It is based on the characteristics of reflectivity of snow in visible and shortwave infrared (SWIR) bands. The reflectance of snow pixels are high in visible but low in SWIR. So NDSI was derived to calculate using spectral ratio of the reflectance in visible and SWIR band. Through the spectral analysis of the sea fog and other clouds, it presented that the reflectance of the $R_{0.47\mu m}$ is the highest and the lowest in $R_{2.13\mu m}$. Therefore the NDIS is expressed as equation (3). The threshold for NDSI is described as equation (4);

$$NDSI = \frac{R_{0.47\mu m} - R_{2.13\mu m}}{R_{0.47\mu m} + R_{2.13\mu m}} \tag{3}$$

$$NDSI \leq 0.65 \tag{4}$$

4.1.3 Standard deviation test (STD test)

The texture of sea fog is relatively smooth compare to other clouds like low stratus, mid and high level clouds. It is known with the reason of atmospheric stabilities (Gang et al., 2006, Heo et al, 2008, Wu and Li 2014). The inversion layer formed with upwelling of sea water and the sea surface temperature decrease and the lower atmosphere temperature is cooled and relatively warm air flow into cold sea surface and sea fog is formed (Cho et al., 2000; Heo and Ha, 2004). Due to its smooth texture, sea fog always has small standard deviation value than other clouds, especially in the thermal infrared channel (Wu and Li, 2014). Through the spectral analysis fo the sea fog and other clouds for thermal infrared channel, it was confirmed that the standard deviation difference between sea fog and other clouds was the most apparent at channel 11 μm. Therefore we used standard deviation test with brightness temperature of MODIS band 31 (11 μm) data to discriminate sea fog from other clouds. Various sizes of moving window of 3 km x 3 km, 7 km x 7 km, 15 km x 15 km, 31 km x 31 km, 71 km x 71 km and 101 km x 101 km were used with various thresholds of 0.5 to 3 with interval of 0.5 was used to decide the most optimal one. The threshold for standard deviation test is expressed as equation (5).

$$\sigma_{IR} \leq 1K \quad (5)$$

4.1.4 Temperature difference index (TDI)

We calculated the temperature difference index (TDI) by calculating the brightness temperature of cloud top (BT_{cloud_top}) minus sea surface temperature (SST) to discriminate between the sea fog and stratus cloud. When sea fog is occurred there is inversion profile presence. Therefore, the sea temperature gets cold and the cloud top temperature increases. As the result, the difference between the brightness temperature of the sea fog and the sea surface temperature is small when the difference between the brightness temperature of stratus and the sea surface temperature is big. The similarity of them is also due to the low altitude of sea fog compared to stratus, because the top height of sea fog is less than 1 km above the sea surface. The threshold for TDI is expressed as equation (7);

$$TDI = BT_{cloud\,top} - SST \qquad (6)$$

$$TDI \leq 0 \qquad (7)$$

4.1.5 Normalized water vapor index (NWVI)

Finally, as the last step of the algorithm, we applied the Normalized Water Vapor Index (NWVI) using the MODIS near-infrared water vapor absorption bands (Band 17: 904 nm and Band 18: 936 nm) to remove the least of the stratus area. The NWVI is expressed as in equation (8) and the threshold can be applied. The threshold for NWVI in spring season is expressed as equation (9);

$$NWVI = \frac{R_{0.93\mu m} - R_{0.90\mu m}}{R_{0.93\mu m} + R_{0.90\mu m}} \tag{8}$$

$$NWVI \leq -0.2 \tag{9}$$

As shown in the equation (8), The Normalized Water Vapor Index is calculated using the channel 17 (904 nm) and channel 18 (936 nm). Channel 17 is the most sensitive to water vapor and channel 18 is the least sensitive. Therefore, the NWVI value of sea fog is much lower than the NWVI value of other clouds.

4.2 Validation method of detection result

To validate the detection, COMS/MI and GOCI image is used to verify wjether or not there is an actual sea fog. The detection results are shown on the top of false color composite image in red closed line to compare directly. The COMS/MI fog product is compared visually using the closest time of observation. Due to high temporal resolution of MI image, it was easier to confirm the cases.

4.3 Threshold decision method

To find more suitable threshold value for each index, we first tried some range of threshold to each index then calculated the Hanssen-Kuiper Skill Score (KSS) through the probability of detection (POD) value and false alarm rate (FAR) using the algorithm detection result and manual detection result. The equation of KSS is expressed as equation (10). After applying the NDSI index, we applied threshold range from 0.4 to 0.9 with interval of 0.05 according to the spectral test to distinguish other clouds from cloudy area. According to the KSS result, we decided the higher value of the KSS until it increase significantly. After the decision of threshold value for the NDSI, we proceed to the next step, the STD test with various window sizes and threshold. Then, the KSS value of STD test for threshold range from -1 to 3. The higher KSS value with significant increase was decided to be the most suitable threshold.

Table 7. The Contingency Table.

A: Hits, B: False alarm, C: Misses, D: Correct Negatives

	Manual detection **Yes**	Manual detection **No**
Algorithm detection **Yes**	A	B
Algorithm detection **No**	C	D

$$KSS = POD - FAR = \frac{A}{A+C} - \frac{B}{B+D} \qquad (10)$$

4.4 Test result using visible channel data (GOCI)

As mentioned in the previous section, GOCI has great potential in terms of detecting sea fog because of higher frequency of observation. However there is no enough studies on detecting sea fog using visible and NIR. In 2016, there was study published about sea fog detection using GOCI (Yuan et al., 2016). The algorithm explained in the paper about the base thesis. Fig. 16 show sthe result of the detection result using the algorithm presented in Yuan et al. (2016). Fig. 19 (a) is presenting the sea fog area in white dot and (b) is showing the same detection result on the RGB color composite image.

According to the previous paper, GOCI L1B data is converted to Rayleigh corrected reflectance and then discriminated land and sea area using sea - land discrimination index (SLDI, expressed as equation (11). Then applied middle/high level cloud deduction index (MCDI) whih can be expressed as equation (12). After deducting middle/high level clouds, sea fog and low stratus are left and to remove low stratus, the band slope index (BSI) was applied which can be applied as equation (13).

$$SLDI = \frac{R_{865nm} - R_{555nm}}{R_{865nm} + R_{555nm}} \tag{11}$$

$$MCDI = \sum_{i=1}^{8} R_{band(i)} / 8 \tag{12}$$

$$BSI = (R_{745nm} - R_{680nm}) / \triangle nm \, \mathrm{x} \, 10\, \mathrm{e}^{4} \tag{13}$$

While using GOCI data, some error lines were found in the image. Through the discussion with the GOCI operation team, it was confirmed that there is error occurred during the geometric correction process. Yet they have no found the solution and it is expected to be fixed on the next generation of GOCI. With this kind of matters, the accuracy of the sea fog detection result using GOCI is low.

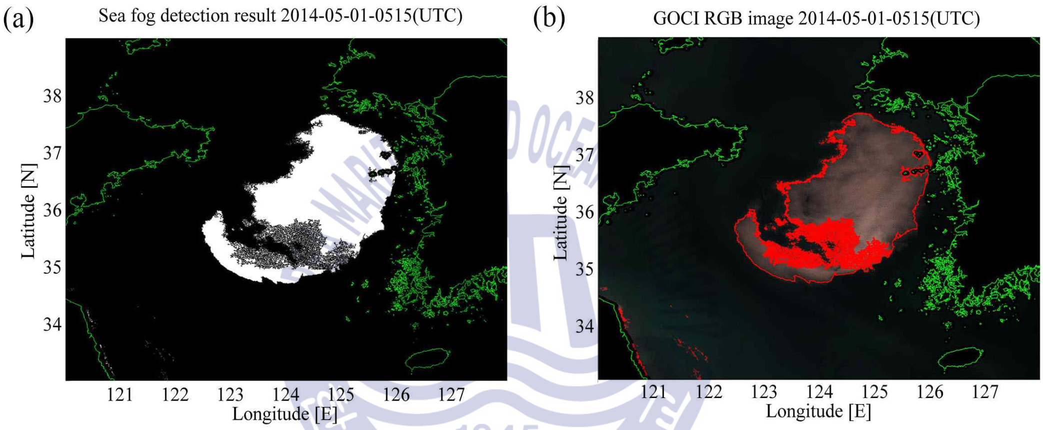

Fig. 19 Sea fog detection result using Yuan et al., (2016) algorithm with Rayleigh corrected GOCI reflectance data for test. The result is presented in (a) white dots and (b) red closed line on the RGB image

Chapter 5. Results and Discussion

5.1 Detection result using improved detection method

The previous daytime sea fog detection algorithm developed by Wu and Li (2014) is designed to use Terra/MODIS data and NDSI. It is calculated using Band 6 (1.64 μm) and Band 1 (0.65 μm). However in Aqua/MODIS band 6, there are 15 out of 20 inoperable detectors which results some failure in detection using Aqua/MODIS data. Due to this, there were some problem in the detection result when the algorithm is applied to Aqua/MODIS data set.

Also, on the pre-processing step, we found that the land mask results were showing that some land is still unmasked even after the process. To solve this problem, we masked with 10 km buffered land mask image and finally all land area were able to be masked. However, the disadvantage of this process is that it also can remove sea fog areas occurring near coast.

Using the improved algorithm, the results of cloud mask application are shown in Fig. 20 - Fig. 28 (a). The result shows that the results often include non-cloud regions.

Using the NDSI, the non-cloud regions were eliminated as well as some parts of mid/high clouds. The result is shown in Fig. 20 - Fig. 28 (b). The NDSI result shows significant removal of non- cloud area. Also we have tried with various threshold values from 0.4 to 0.9 with interval of 0.05 mainly to detect cloud and to remove the non-cloud area from the cloud mask result. As shown in Table 5, the highest score was shown when the NSDI threshold of 0.8 was used. However, there were less increase since the threshold of 0.65 and therefore, the final NDSI threshold was decided as 0.65.

For standard deviation test, we have applied to find more suitable size of window to calculate standard deviation, by trying the window size of 3, 7, 31, 71 and 101. We also tried various threshold values from 0.5 to 2.5 with interval of 0.5. The KSS of each threshold values using various sizes of windows are shown in Table 6. The highest KSS was derived when, window size of 101 was used. Also, the threshold of 1 was showing the highest KSS.

After the STD test, we tried to eliminate the stratus using the BTCT-SST test result shown in Fig. 20 – Fig. 28 (d). To derive better threshold the index was appled and tested with threshold value of −1 to 3 as shown in Table 7. The highest KSS was derived when threshold value of 1 was used.

Lastly, NWVI was tested with threshold value of −0.1 to −0.4. The highest KSS was derived when using threshold value of −0.2 as shown in Table 8. The final result is overlaied on RGB color composite image using Band 6, 2, 1 in red closed line in Fig. 20 – Fig. 28 (f).

The final detection result using training data is shown in Fig. Fig. 20 – Fig. 28. Fig. 20 to 26 shows KSS value of higher than 0.97. Fig 27 and 28 shows some miss of detection. The improved algorithm using test data is showing promising result as the average KSS result is 0.74.

Fig. 29 and 30 are showing that all sea fog areas are perfectly detected. Fig. 31 and 32 are showing that all sea fog areas are detected, but also detected some non-cloud areas and cloudy areas. More clouds are detected as well as all sea fog areas in Fig. 33. However there are some cases like Fig. 34 and 35 which are showing that they have detected many non-cloud areas and missed some of the sea fog areas. Fig. 37 indicates it have discriminated other clouds and only detected sea fog areas.

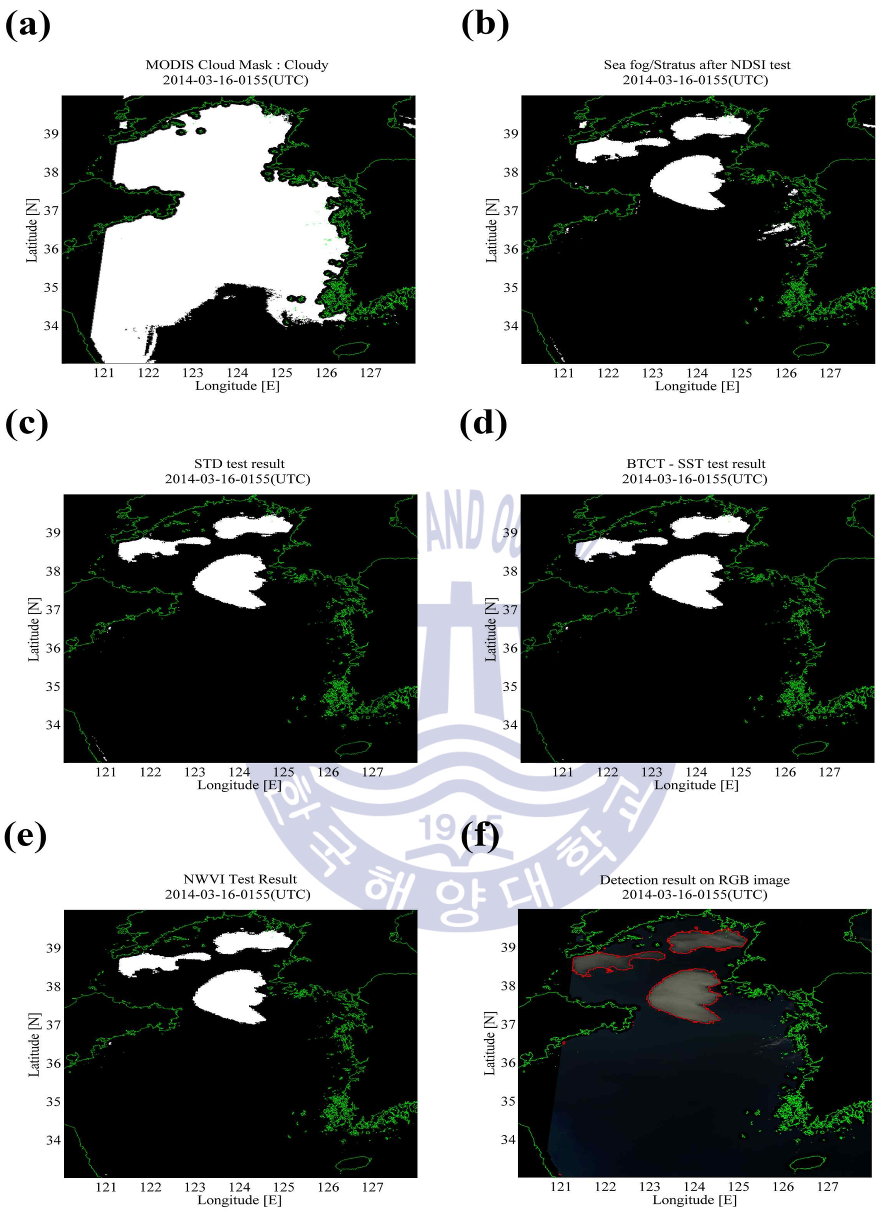

Fig. 20 Result of sea fog detection procedure using Terra/MODIS on 2014-March-16 01:55 (UTC). The result after (a) the MODIS Cloud Mask application (Cloudy), (b) the NDSI result, (c) the STD test, (d) the BTCT-SST index, (e) the NWVI test, (f) the final sea fog detection result in red closed line on RGB color composite image

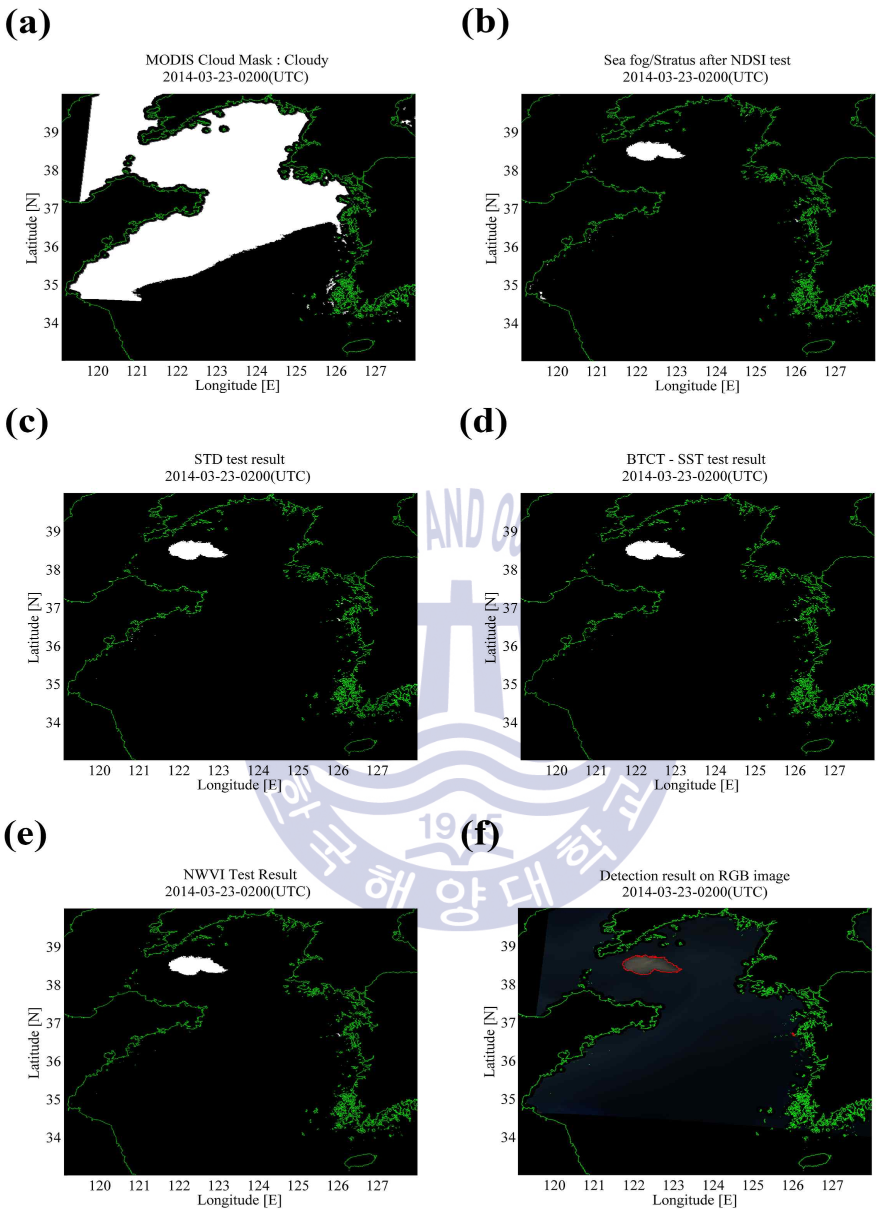

Fig. 21 Result of sea fog detection procedure using Terra/MODIS on 2014-March-23 02:00 (UTC). The result after (a) the MODIS Cloud Mask application (Cloudy), (b) the NDSI result, (c) the STD test, (d) the BTCT-SST index, (e) the NWVI test, (f) the final sea fog detection result in red closed line on RGB color composite image

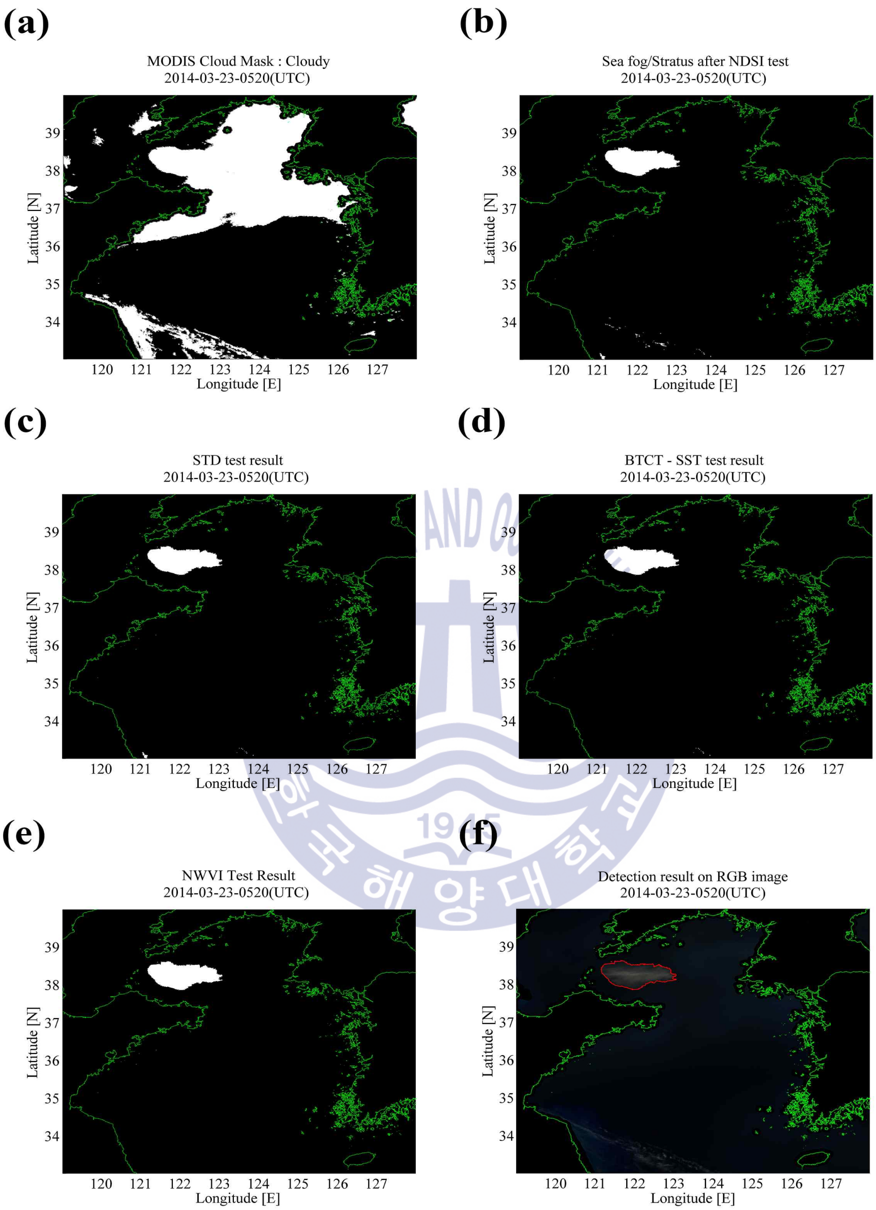

Fig. 22 Result of sea fog detection procedure using Aqua/MODIS on 2014-March-23 05:20 (UTC). The result after (a) the MODIS Cloud Mask application (Cloudy), (b) the NDSI result, (c) the STD test, (d) the TDI index, (e) the NWVI test, (f) the final sea fog detection result in red closed line on RGB color composite image

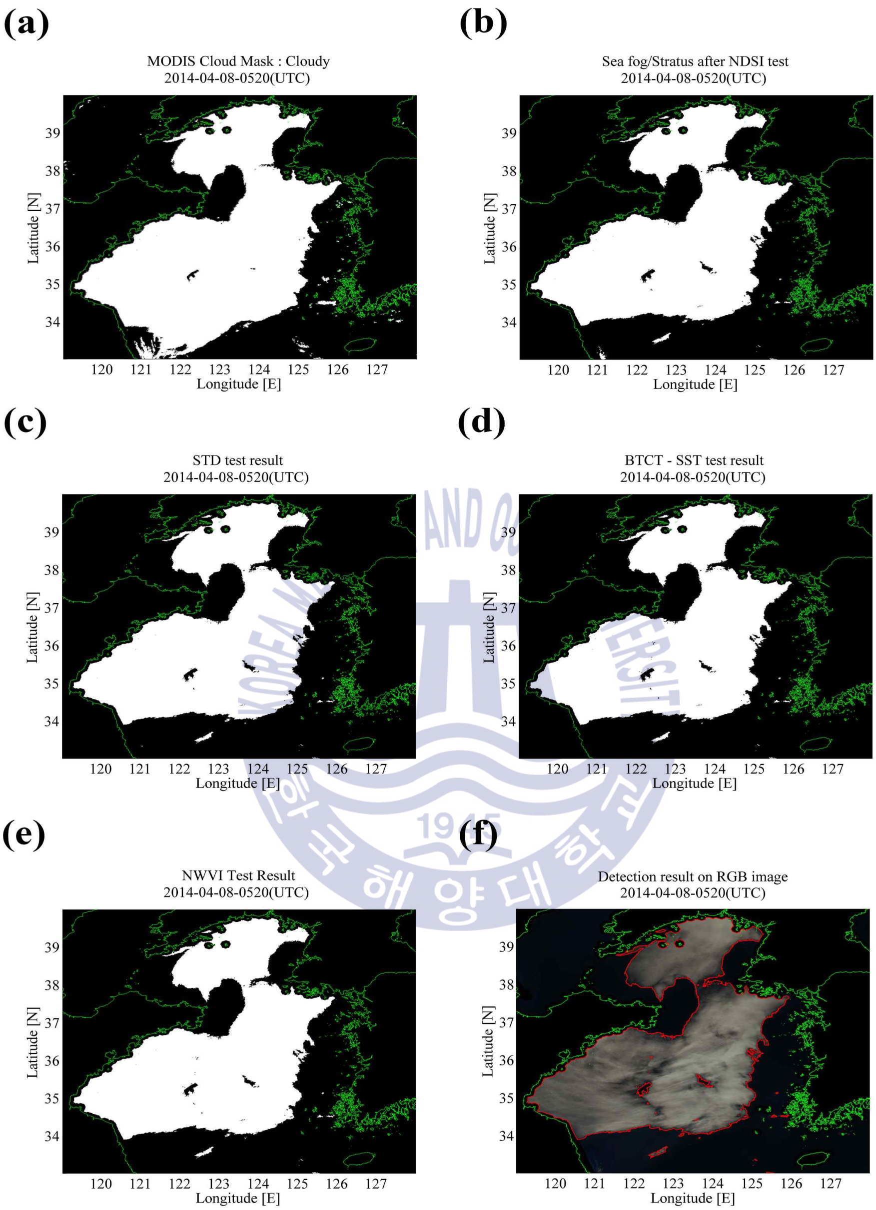

Fig. 23 Result of sea fog detection procedure using Aqua/MODIS on 2014-April-08 05:20 (UTC). The result after (a) the MODIS Cloud Mask application (Cloudy), (b) the NDSI result, (c) the STD test, (d) the TDI index, (e) the NWVI test, (f) the final sea fog detection result in red closed line on RGB color composite image

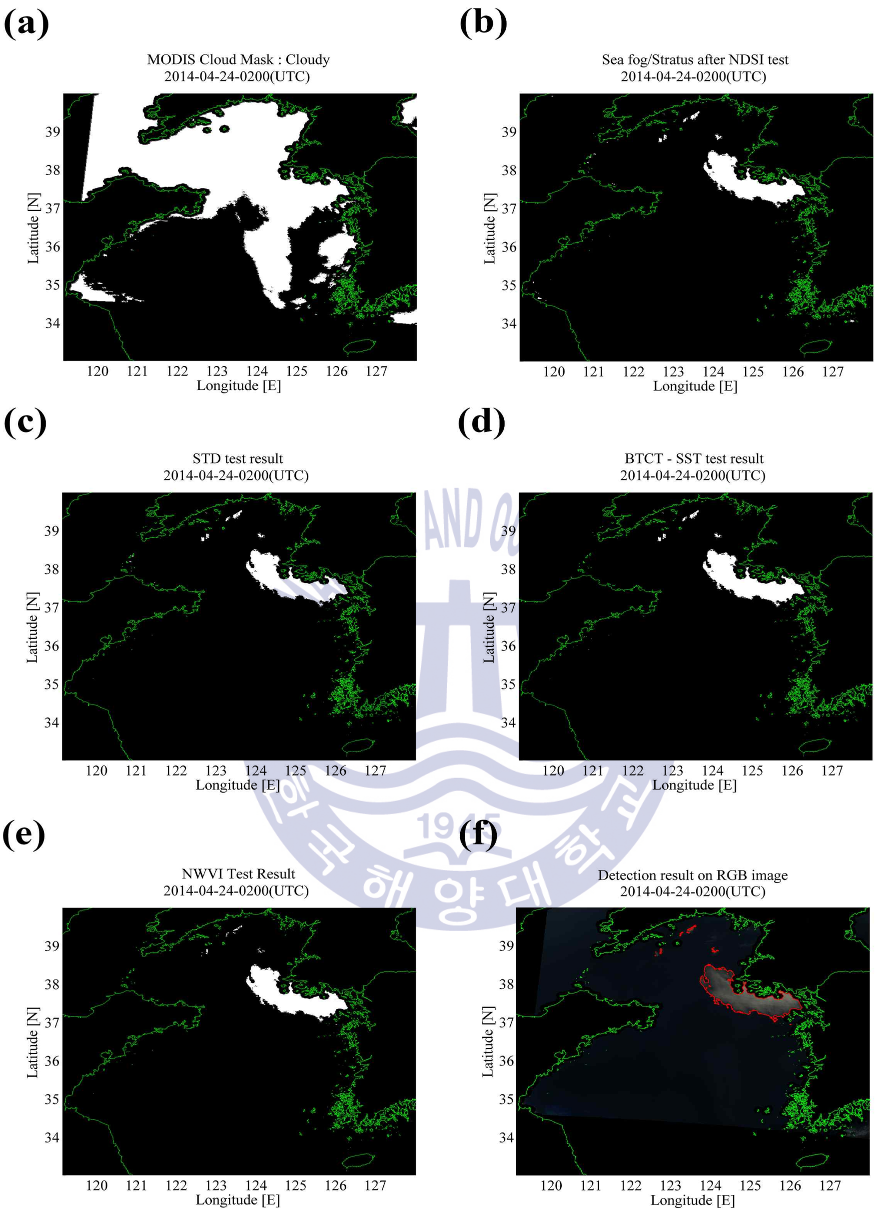

Fig. 24 Result of sea fog detection procedure using Terra/MODIS on 2014-April-24 02:00 (UTC). The result after (a) the MODIS Cloud Mask application (Cloudy), (b) the NDSI result, (c) the STD test, (d) the TDI index, (e) the NWVI test, (f) the final sea fog detection result in red closed line on RGB color composite image

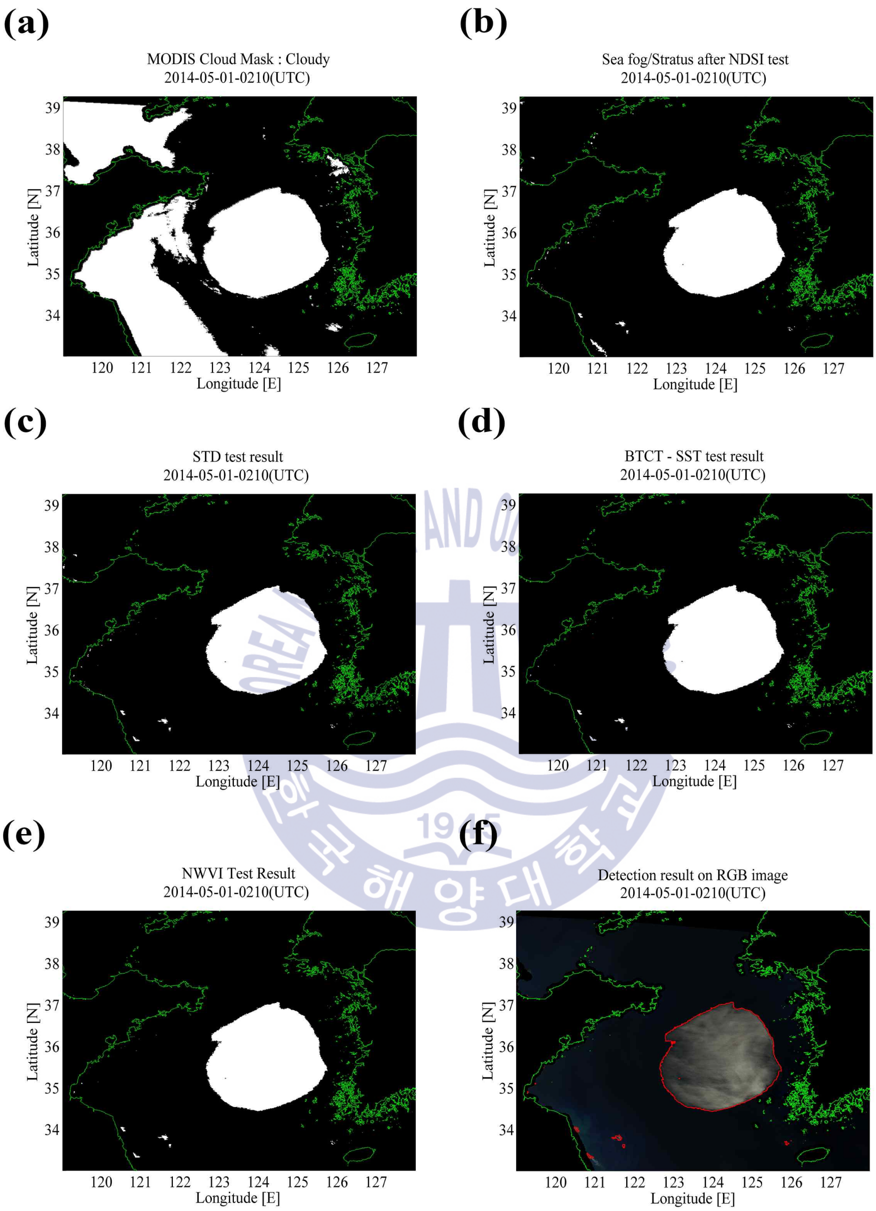

Fig. 25 Result of sea fog detection procedure using Terra/MODIS on 2014-May-01 02:10 (UTC). The result after (a) the MODIS Cloud Mask application (Cloudy), (b) the NDSI result, (c) the STD test, (d) the TDI index, (e) the NWVI test, (f) the final sea fog detection result in red closed line on RGB color composite image

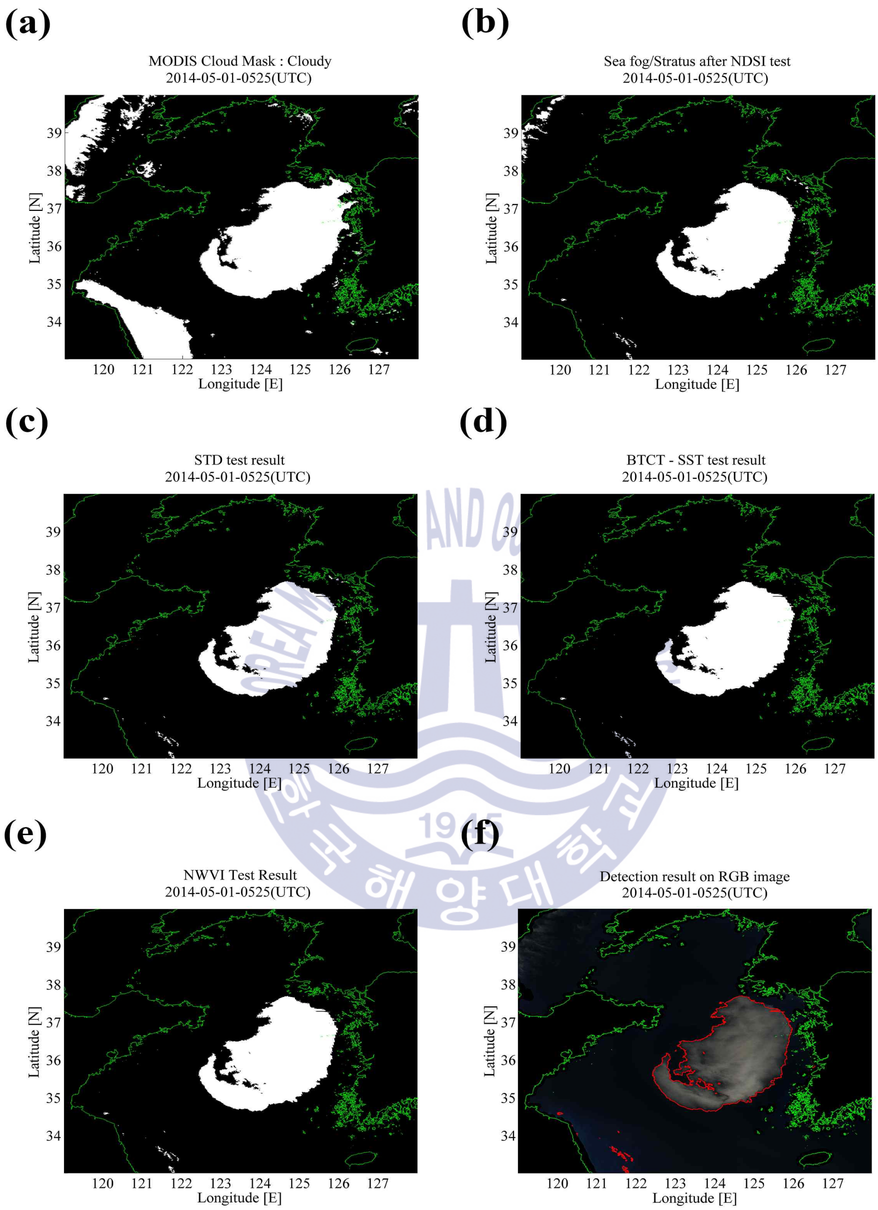

Fig. 26 Result of sea fog detection procedure using Aqua/MODIS on 2014-May-01 05:25 (UTC). The result after (a) the MODIS Cloud Mask application (Cloudy), (b) the NDSI result, (c) the STD test, (d) the TDI index, (e) the NWVI test, (f) the final sea fog detection result in red closed line on RGB color composite image

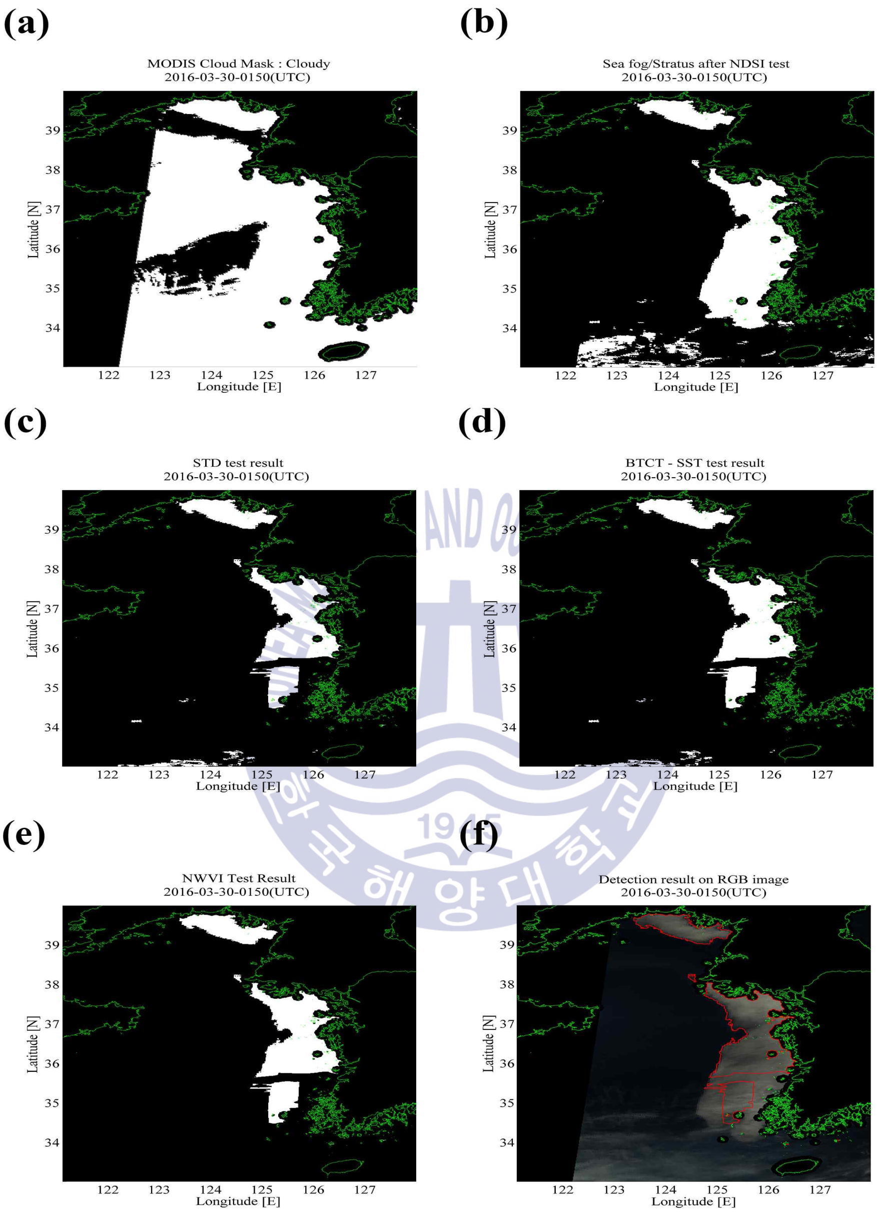

Fig. 27 Result of sea fog detection procedure using Terra/MODIS on 2016-March-30 01:50 (UTC). The result after (a) the MODIS Cloud Mask application (Cloudy), (b) the NDSI result, (c) the STD test, (d) the TDI index, (e) the NWVI test, (f) the final sea fog detection result in red closed line on RGB color composite image

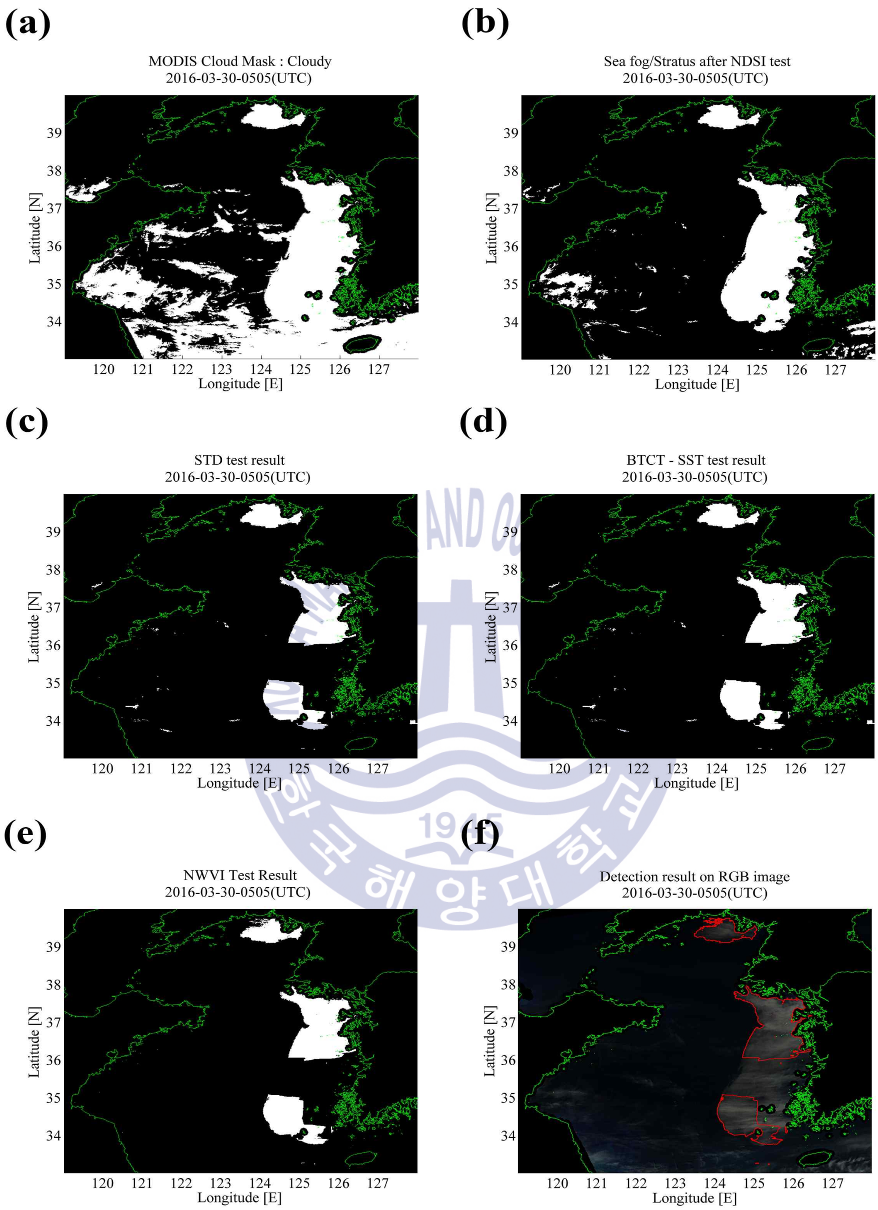

Fig. 28 Result of sea fog detection procedure using Aqua/MODIS on 2016-March-30 05:05 (UTC). The result after (a) the MODIS Cloud Mask application (Cloudy), (b) the NDSI result, (c) the STD test, (d) the TDI index, (e) the NWVI test, (f) the final sea fog detection result in red closed line on RGB color composite image

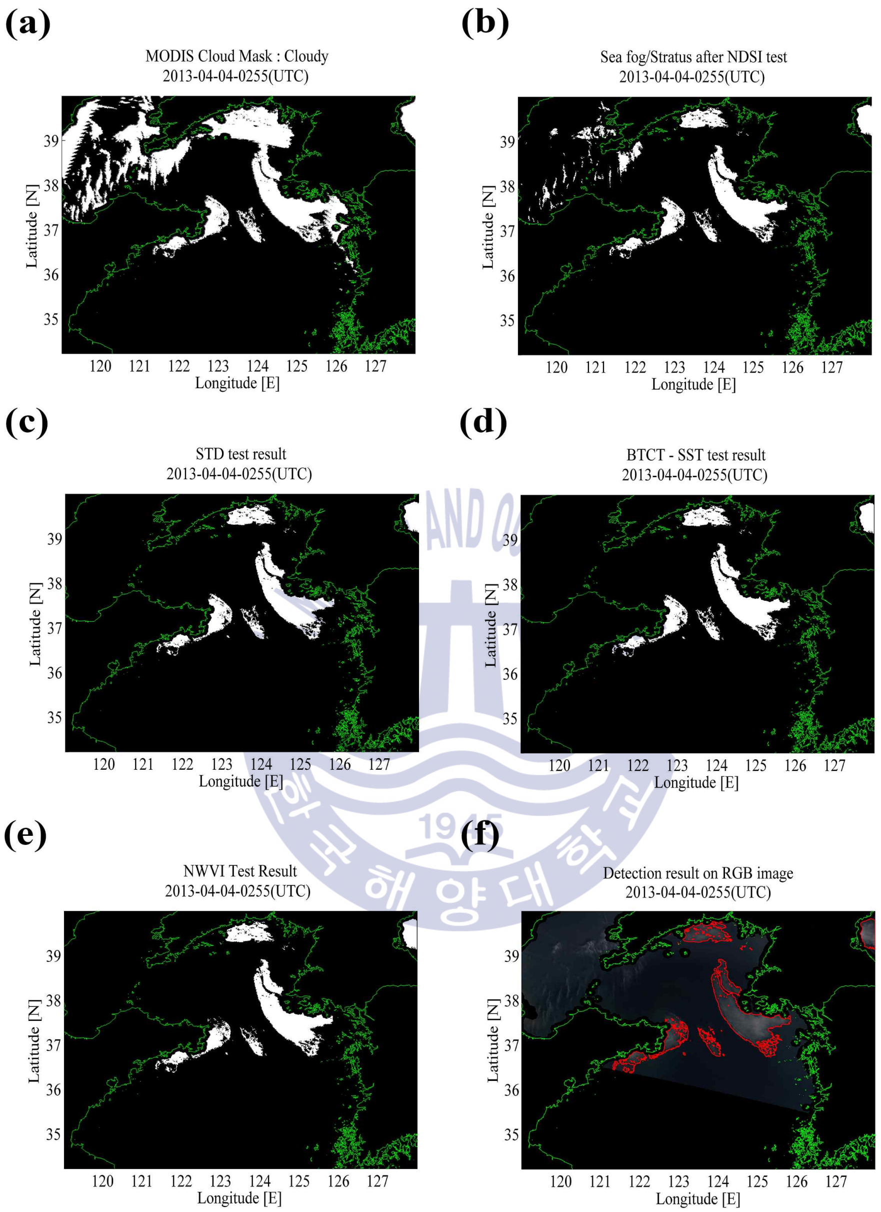

Fig. 29 Result of sea fog detection procedure using Terra/MODIS on 2013-April-04 02:55 (UTC). The result after (a) the MODIS Cloud Mask application (Cloudy), (b) the NDSI result, (c) the STD test, (d) the TDI index, (e) the NWVI test, (f) the final sea fog detection result in red closed line on RGB color composite image

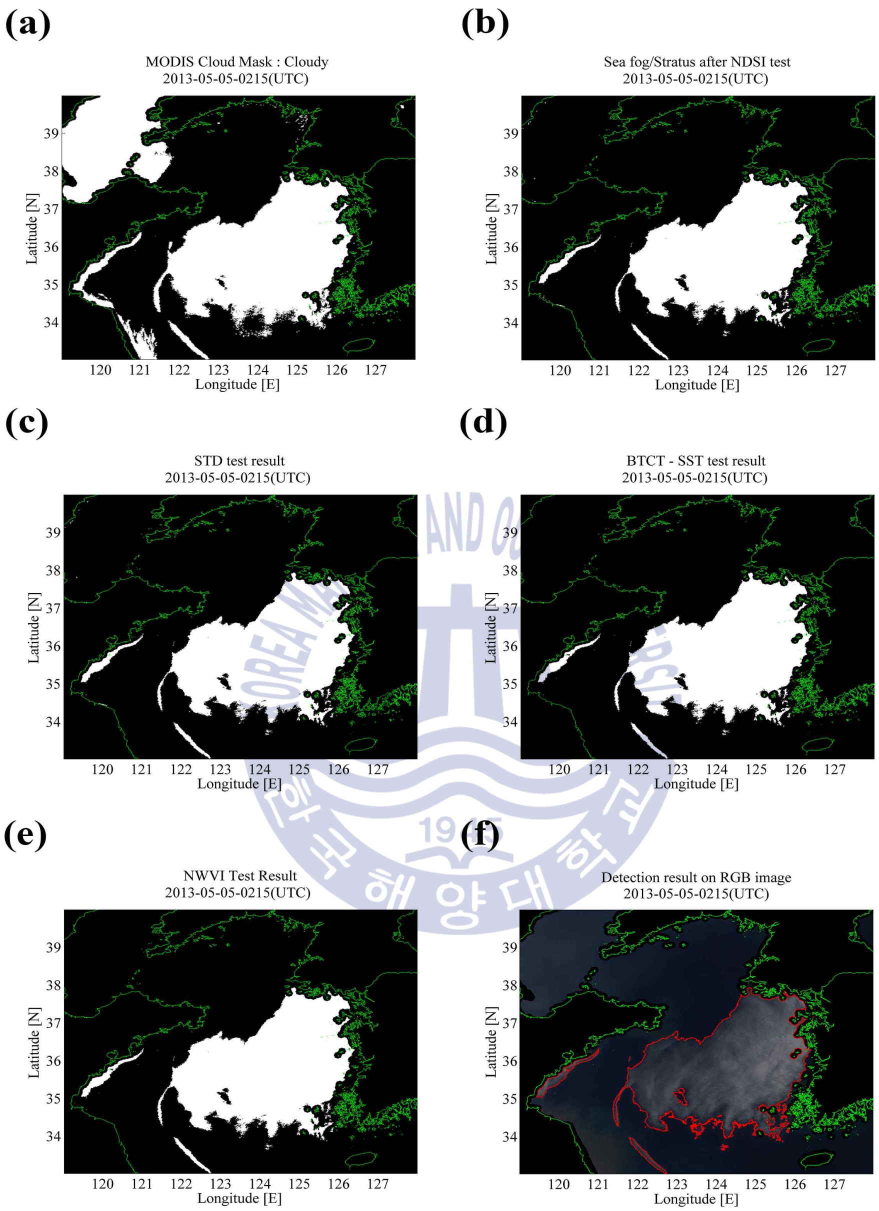

Fig. 30 Result of sea fog detection procedure using Terra/MODIS on 2013-March-05 02:15 (UTC). The result after (a) the MODIS Cloud Mask application (Cloudy), (b) the NDSI result, (c) the STD test, (d) the TDI index, (e) the NWVI test, (f) the final sea fog detection result in red closed line on RGB color composite image

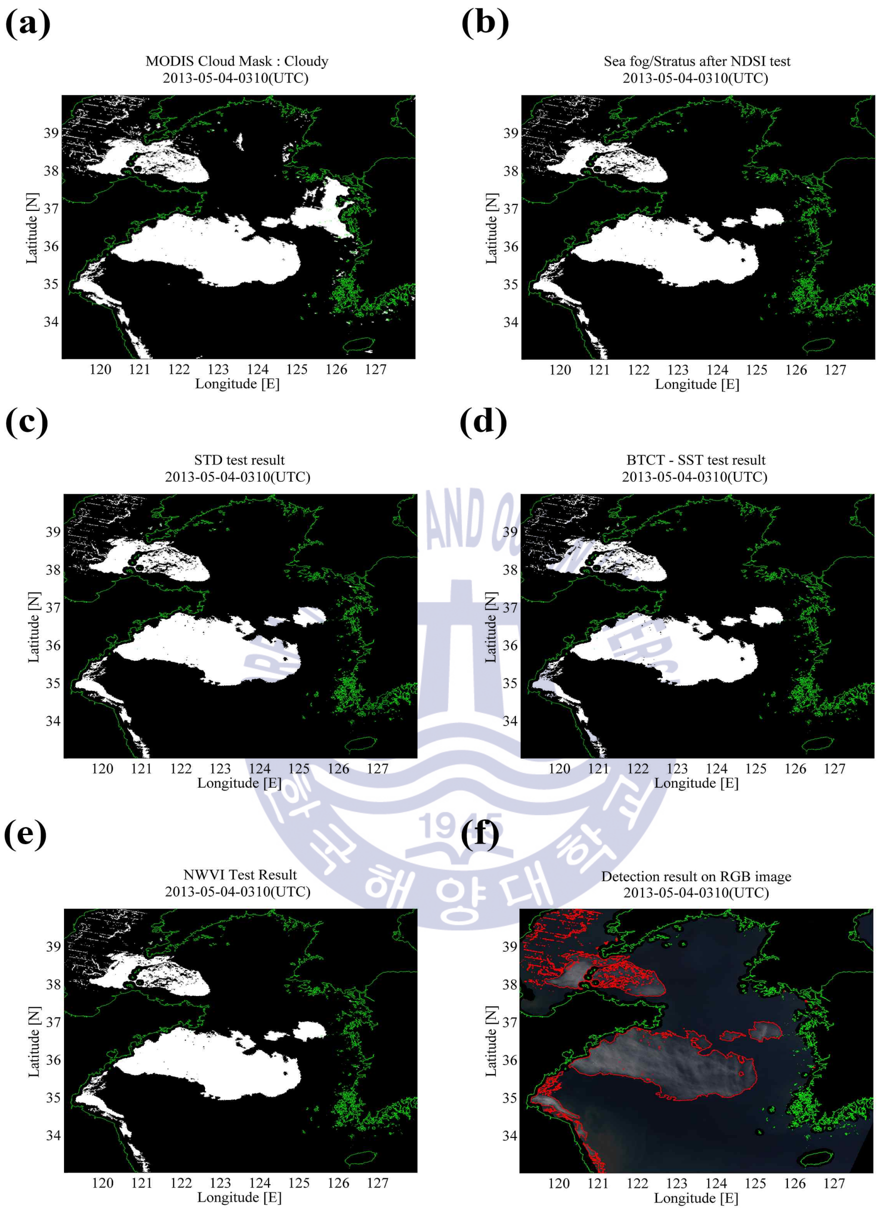

Fig. 31 Result of sea fog detection procedure using Terra/MODIS on 2013-May-04 03:10 (UTC). The result after (a) the MODIS Cloud Mask application (Cloudy), (b) the NDSI result, (c) the STD test, (d) the TDI index, (e) the NWVI test, (f) the final sea fog detection result in red closed line on RGB color composite image

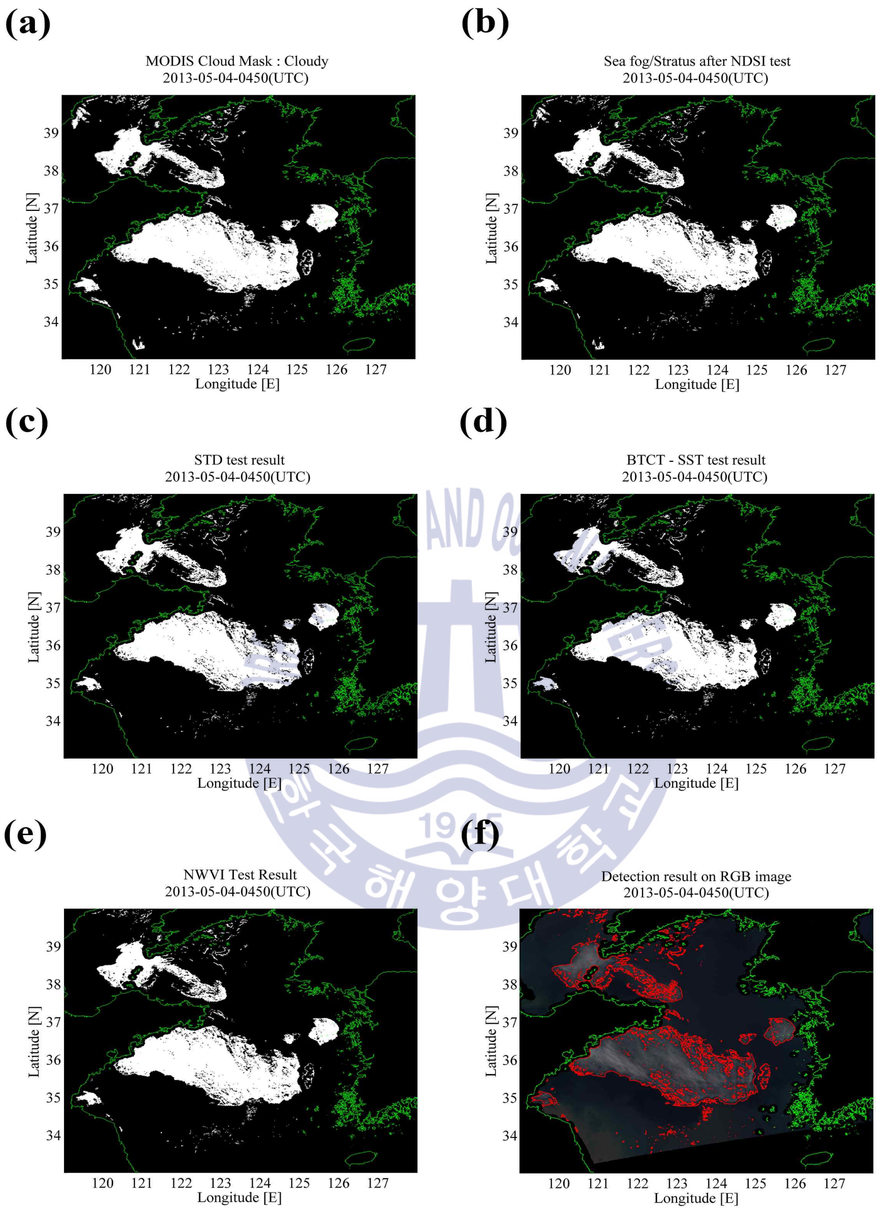

Fig. 32 Result of sea fog detection procedure using Aqua/MODIS on 2013-May-04 04:50 (UTC). The result after (a) the MODIS Cloud Mask application (Cloudy), (b) the NDSI result, (c) the STD test, (d) the TDI index, (e) the NWVI test, (f) the final sea fog detection result in red closed line on RGB color composite image

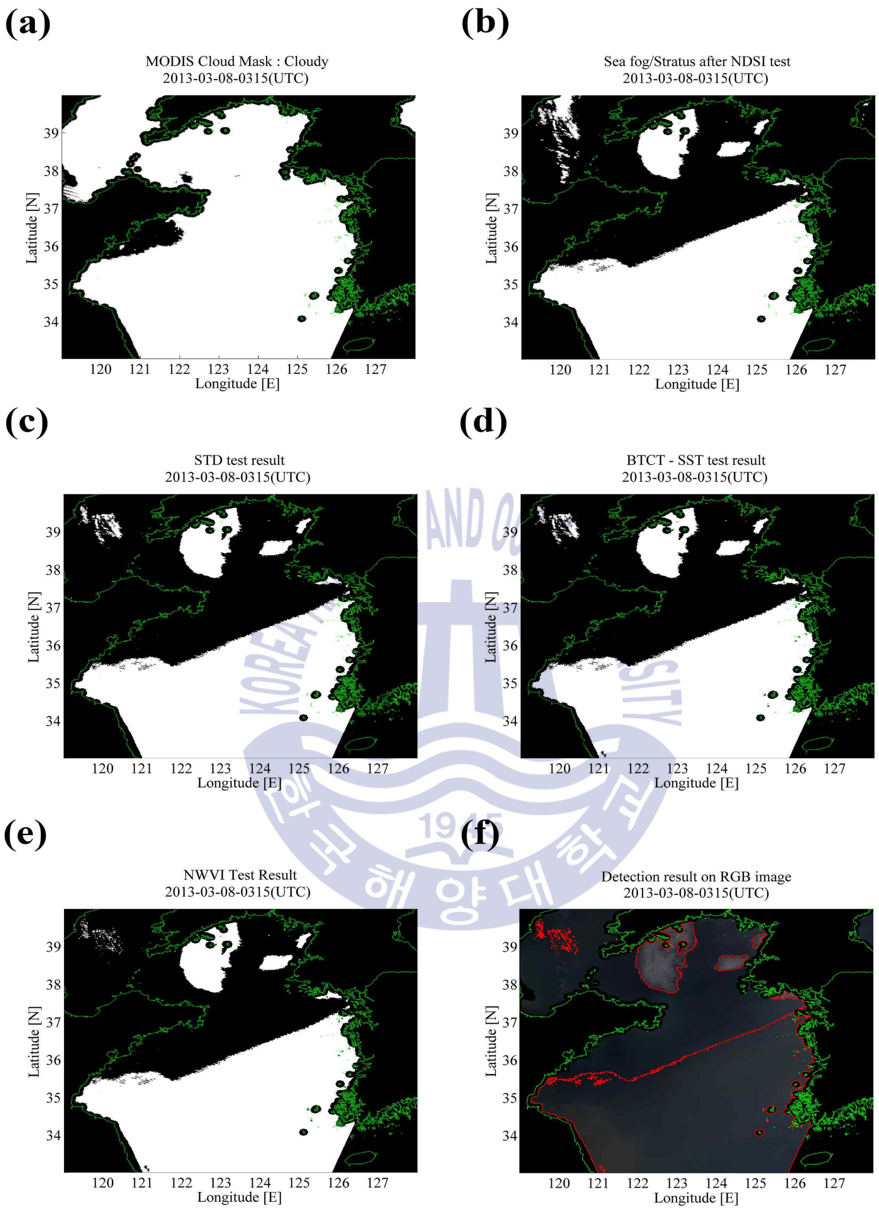

Fig. 33 Result of sea fog detection procedure using Terra/MODIS on 2013-March-08 03:15 (UTC). The result after (a) the MODIS Cloud Mask application (Cloudy), (b) the NDSI result, (c) the STD test, (d) the TDI index, (e) the NWVI test, (f) the final sea fog detection result in red closed line on RGB color composite image

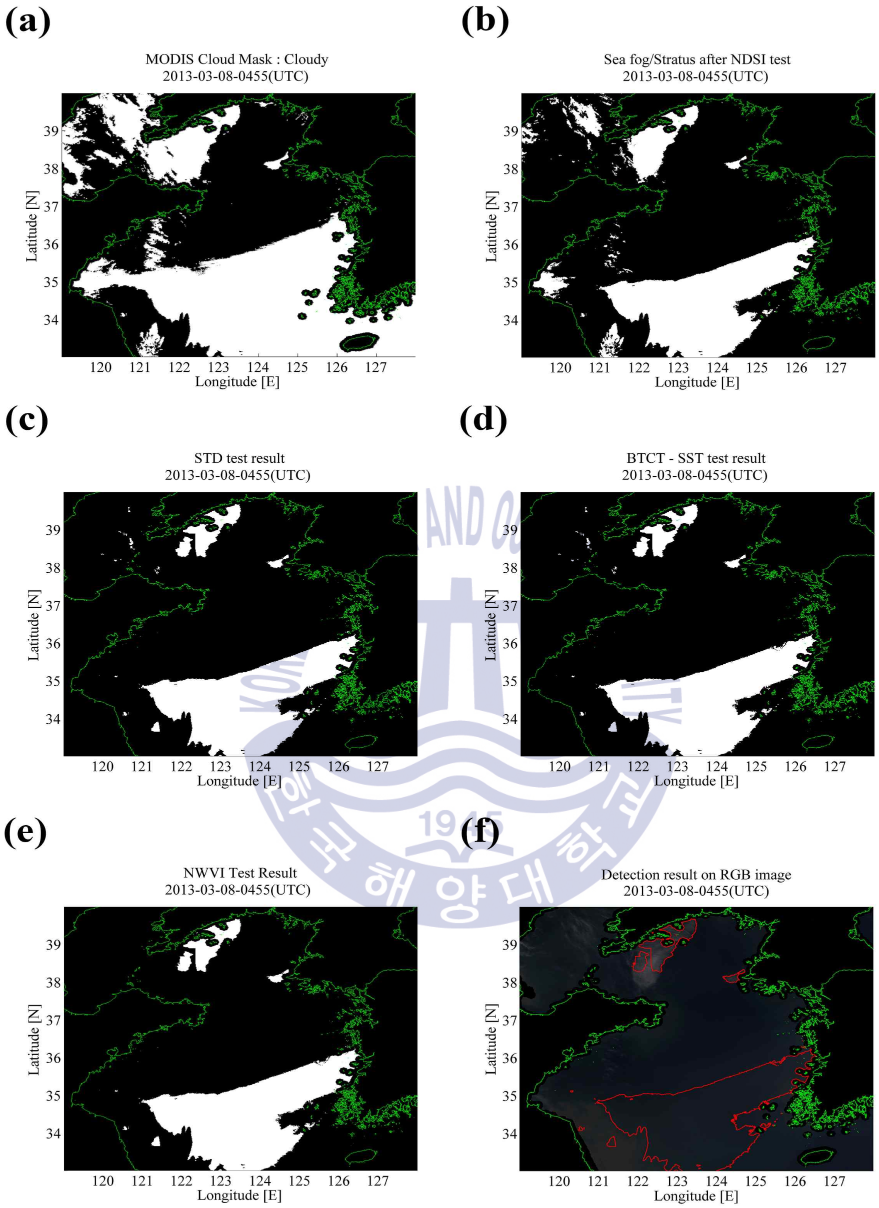

Fig. 34 Result of sea fog detection procedure using Aqua/MODIS on 2013-March-08 04:55 (UTC). The result after (a) the MODIS Cloud Mask application (Cloudy), (b) the NDSI result, (c) the STD test, (d) the TDI index, (e) the NWVI test, (f) the final sea fog detection result in red closed line on RGB color composite image

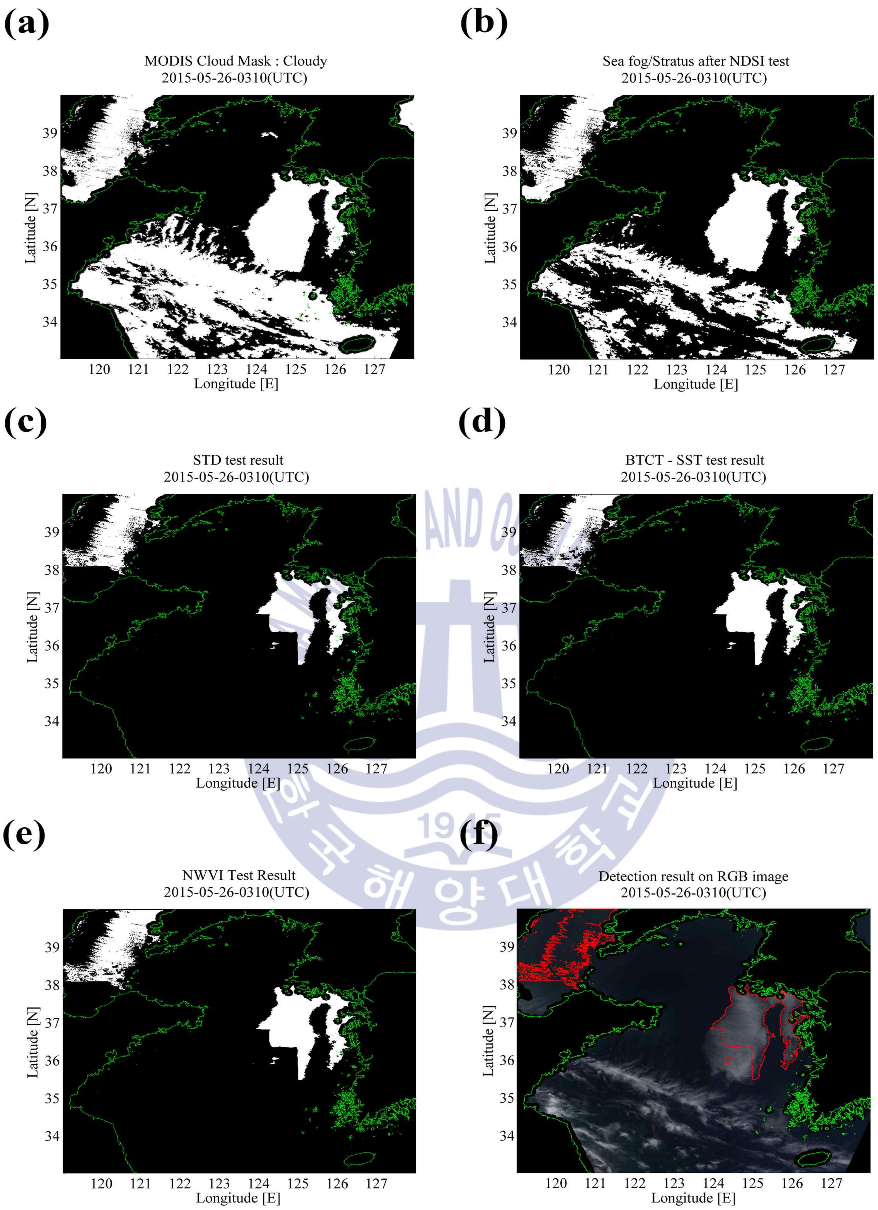

Fig. 35 Result of sea fog detection procedure using Terra/MODIS on 2015-May-26 03:10 (UTC). The result after (a) the MODIS Cloud Mask application (Cloudy), (b) the NDSI result, (c) the STD test, (d) the TDI index, (e) the NWVI test, (f) the final sea fog detection result in red closed line on RGB color composite image

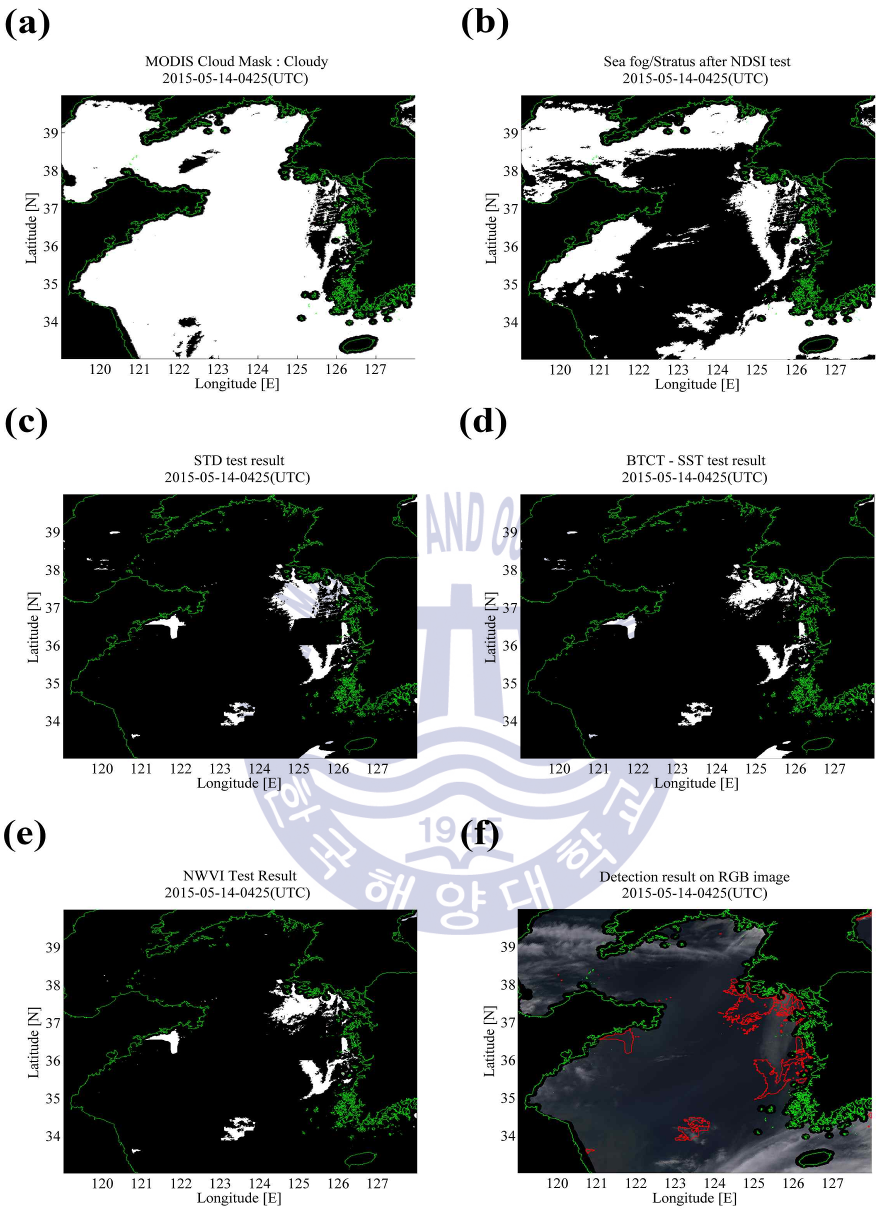

Fig. 36 Result of sea fog detection procedure using Aqua/MODIS on 2015-May-14 04:25 (UTC). The result after (a) the MODIS Cloud Mask application (Cloudy), (b) the NDSI result, (c) the STD test, (d) the TDI index, (e) the NWVI test, (f) the final sea fog detection result in red closed line on RGB color composite image

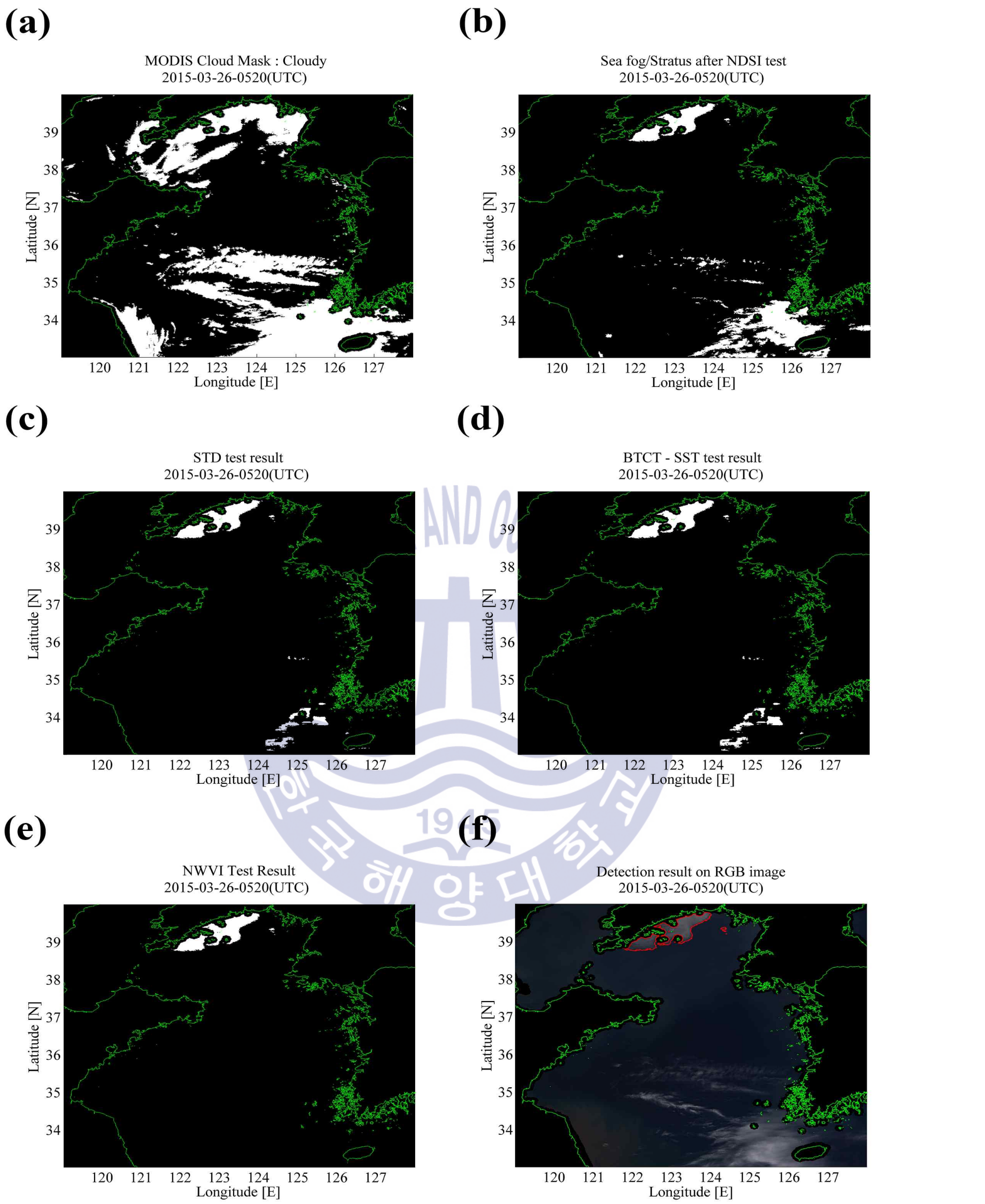

Fig. 37 Result of sea fog detection procedure using Aqua/MODIS on 2015-March-26 05:20 (UTC). The result after (a) the MODIS Cloud Mask application (Cloudy), (b) the NDSI result, (c) the STD test, (d) the TDI index, (e) the NWVI test, (f) the final sea fog detection result in red closed line on RGB color composite image

Table 8. The Hanssen- Kuiper Skill Score of detection result using NDSI threshold for nine training data set (Table 4)

Threshold	2014.03.16 01:55	2014.03.23 02:00	2014.03.23 05:20	2014.04.08 05:20	2014.04.24 02:00	2014.05.01 02:10	2014.05.01 05:25	2016.03.30 01:50	2016.03.30 05:05
0.4	0.845	0.828	0.788	0.975	0.819	0.954	0.903	0.907	0.833
0.45	0.874	0.85	0.88	0.983	0.866	0.975	0.934	0.934	0.9
0.5	0.892	0.876	0.954	0.987	0.904	0.985	0.956	0.952	0.942
0.55	0.909	0.905	0.986	0.989	0.939	0.992	0.975	0.965	0.966
0.6	0.928	0.928	0.993	0.99	0.964	0.994	0.983	0.97	0.972
0.65	0.941	0.944	0.994	0.99	0.982	0.994	0.983	0.955	0.96
0.7	0.954	0.969	0.993	0.989	0.994	0.993	0.978	0.913	0.935
0.75	0.97	0.987	0.989	0.987	0.993	0.992	0.971	0.875	0.897
0.8	0.968	0.994	0.985	0.983	0.981	0.989	0.963	0.84	0.855
0.85	0.824	0.85	0.929	0.959	0.963	0.926	0.916	0.709	0.821
0.9	0.686	0.726	0.833	0.934	0.831	0.778	0.903	0.66	0.816

Table 9 The Hanssen- Kuiper Skill Score (KSS) of detection result using STD threshold with window size of 3, 7, 15, 31, 71 and 101 with the threshold of 0.5 to 3 for training dataset. The “WS” indicates the window size used for STD test

Data	2014.03.16. 01:55						2014.03.23. 02:00						2014.03.23. 05:20					
WS	3	7	15	31	71	101	3	7	15	31	71	101	3	7	15	31	71	101
0.5	0.791	0.797	0.798	0.798	0.799	0.799	0.806	0.806	0.806	0.806	0.806	0.806	0.990	0.989	0.989	0.989	0.989	0.989
1	0.930	0.937	0.940	0.940	0.940	0.940	0.944	0.944	0.944	0.944	0.944	0.944	0.994	0.994	0.994	0.994	0.994	0.994
1.5	0.922	0.941	0.941	0.941	0.941	0.941	0.944	0.944	0.944	0.944	0.944	0.944	0.994	0.994	0.994	0.994	0.994	0.994
2	0.920	0.941	0.941	0.941	0.941	0.941	0.944	0.944	0.944	0.944	0.944	0.944	0.994	0.994	0.994	0.994	0.994	0.994
2.5	0.846	0.941	0.941	0.941	0.941	0.941	0.944	0.944	0.944	0.944	0.944	0.944	0.995	0.994	0.994	0.994	0.994	0.994
3	0.799	0.941	0.941	0.941	0.941	0.941	0.944	0.944	0.944	0.944	0.944	0.944	0.995	0.994	0.994	0.994	0.994	0.994
Data	2014.04.08. 05:20						2014.04.24. 02:00						2014.05.01. 02:10					
WS	3	7	15	31	71	101	3	7	15	31	71	101	3	7	15	31	71	101
0.5	0.981	0.981	0.981	0.981	0.981	0.981	0.948	0.948	0.948	0.948	0.948	0.948	0.963	0.962	0.962	0.962	0.962	0.962
1	0.990	0.990	0.990	0.990	0.990	0.990	0.982	0.982	0.982	0.982	0.982	0.982	0.995	0.994	0.994	0.994	0.994	0.994
1.5	0.990	0.990	0.990	0.990	0.990	0.990	0.983	0.982	0.982	0.982	0.982	0.982	0.995	0.994	0.994	0.994	0.994	0.994
2	0.990	0.990	0.990	0.990	0.990	0.990	0.983	0.982	0.982	0.982	0.982	0.982	0.995	0.994	0.994	0.994	0.994	0.994
2.5	0.990	0.990	0.990	0.990	0.990	0.990	0.983	0.982	0.982	0.982	0.982	0.982	0.995	0.994	0.994	0.994	0.994	0.994
3	0.990	0.990	0.990	0.990	0.990	0.990	0.977	0.982	0.982	0.982	0.982	0.982	0.995	0.995	0.994	0.994	0.994	0.994

Table 10 The Hanssen- Kuiper Skill Score (KSS) of detection result using STD threshold with window size of 3, 7, 15, 31, 71 and 101 with the threshold of 0.5 to 3 for nine dataset and the average of nine dataset. The “WS” indicates the window size used for STD test

Data	2014.05.01. 05:25						2016.03.30. 01:50						2016.03.30. 05:05					
WS	3	7	15	31	71	101	3	7	15	31	71	101	3	7	15	31	71	101
0.5	0.945	0.944	0.943	0.942	0.942	0.942	0.730	0.794	0.827	0.841	0.848	0.851	0.843	0.922	0.946	0.954	0.958	0.959
1	0.987	0.986	0.984	0.983	0.983	0.983	0.777	0.895	0.939	0.952	0.955	0.955	0.813	0.915	0.944	0.954	0.958	0.960
1.5	0.987	0.986	0.985	0.984	0.983	0.983	0.717	0.869	0.924	0.945	0.952	0.954	0.731	0.886	0.933	0.948	0.955	0.958
2	0.987	0.986	0.986	0.984	0.983	0.983	0.668	0.822	0.897	0.934	0.951	0.954	0.592	0.842	0.908	0.937	0.953	0.960
2.5	0.986	0.986	0.986	0.984	0.983	0.983	0.587	0.709	0.872	0.924	0.949	0.955	0.397	0.695	0.854	0.939	0.960	0.963
3	0.977	0.983	0.986	0.985	0.983	0.983	0.523	0.672	0.853	0.911	0.950	0.956	0.337	0.590	0.790	0.925	0.963	0.964

Table 11 The Hanssen- Kuiper Skill Score (KSS) of detection result using TDI threshold with the threshold of -1 to 3 for nine training data

Threshold	2014.03.16 01:55	2014.03.23 02:00	2014.03.23 05:20	2014.04.08 05:20	2014.04.24 02:00	2014.05.01 02:10	2014.05.01 05:25	2016.03.30 01:50	2016.03.30 05:05
-1	0.941	0.944	0.979	0.960	0.980	0.995	0.949	0.668	0.581
-0.5	0.941	0.944	0.994	0.983	0.982	0.995	0.981	0.668	0.587
0	0.941	0.944	0.995	0.989	0.982	0.995	0.983	0.668	0.588
0.5	0.941	0.944	0.995	0.990	0.982	0.995	0.983	0.668	0.588
1	0.941	0.944	0.995	0.990	0.982	0.995	0.983	0.668	0.588
1.5	0.940	0.944	0.995	0.990	0.982	0.995	0.983	0.668	0.589
2	0.940	0.944	0.995	0.990	0.982	0.995	0.983	0.668	0.589
2.5	0.940	0.944	0.995	0.990	0.982	0.995	0.983	0.668	0.589
3	0.941	0.944	0.995	0.990	0.982	0.995	0.983	0.668	0.589

Table 12 The Hanssen- Kuiper Skill Score (KSS) of detection result using NWVI threshold with the threshold of −0.1 to −0.4 for nine training data

Threshold	2014.03.16 01:55	2014.03.23 02:00	2014.03.23 05:20	2014.04.08 05:20	2014.04.24 02:00	2014.05.01 02:10	2014.05.01 05:25	2016.03.30 01:50	2016.03.30 05:05
−0.4	0	0	0	0.068	0.536	0.990	0.895	0	0
−0.35	0.322	0.018	0	0.255	0.980	0.995	0.983	0.157	0.005
−0.3	0.935	0.932	0	0.527	0.982	0.995	0.983	0.556	0.265
−0.25	0.941	0.944	0.956	0.867	0.982	0.995	0.983	0.662	0.486
−0.2	0.941	0.944	0.995	0.989	0.982	0.995	0.983	0.673	0.590
−0.15	0.941	0.944	0.995	0.989	0.982	0.995	0.983	0.673	0.589
−0.1	0.941	0.944	0.995	0.989	0.982	0.995	0.983	0.669	0.589

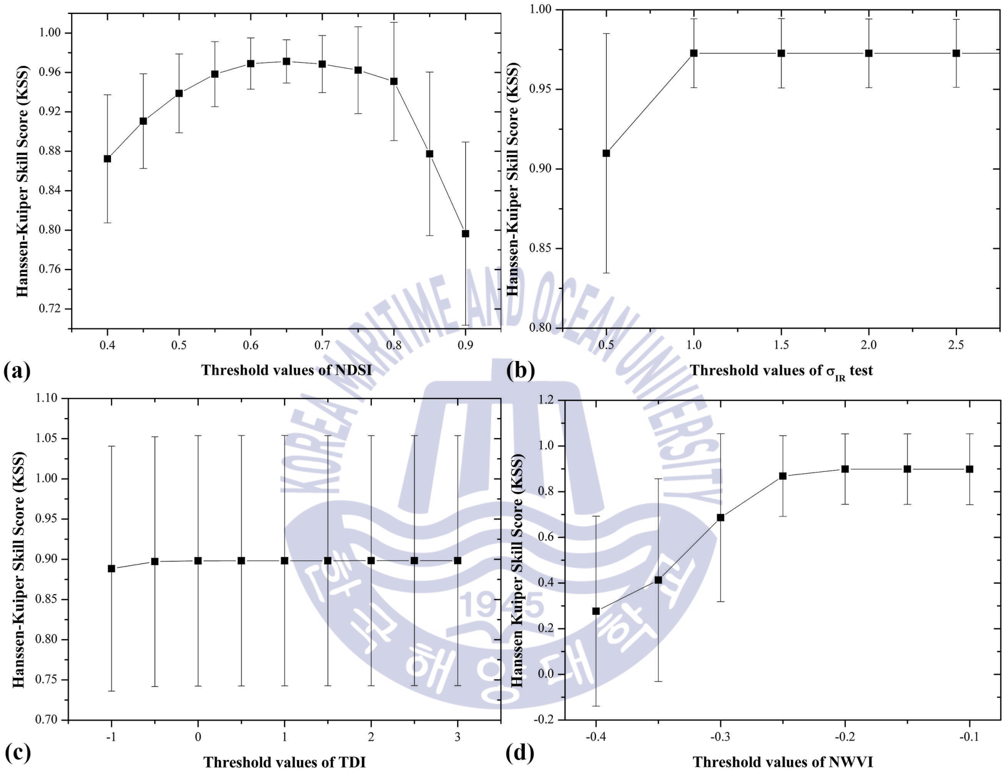

Fig. 38 Average and standard deviation of Hanssen-Kuiper skill score (KSS) with different thresholds for each index. (a) NDSI test, (b) STD test, (c) TDI test, (d) NWVI test

In order to decide the threshold for each index, wide range of threshold was adapted to each index and calculated the average of KSS values (see Table 7). Fig. 38 (a) shows the average and standard deviation KSS values of threshold from 0.4 to 0.9 with interval of 0.05 for NDSI using training data. The highest average KSS value among them is when applied NDSI of 0.65 with average KSS of 0.971 however the only increase was 0.002 from the threshold NDSI of 0.65 with average KSS of 0.969. Therefore the threshold of 0.6 for NDSI was confirmed to be the most suitable to use.

Fig. 38 (b) shows the average and standard deviation KSS values of threshold from 0.5 to 3 with interval of 0.5 for STD with window size of 101 using training data. Before that various window sizes of 3, 7, 15, 31, 71 and 101 to calculate STD with range of threshold and KSS values is calculated (Table 8 and 9) and confirmed that the window size of 101 is showing the biggest KSS value. The highest average KSS value among them is when applied threshold for STD of 1 with 0.973. Compare to other threshold values, it was also showing the biggest difference from the average KSS value of 0.91 with STD of 0.5. Therefore the threshold of 1 for STD was decided to use.

Table 10 shows the KSS value of all nine training data for TDI with threshold from -1 to 3 with interval of 0.5. The average and standard deviation of nine training data is shown in Fig. 38 (C). The highest KSS value was derived when using the threshold of 1. Therefore the threshold of 1 for TDI was decided to use.

Table 11 is showing KSS value of all nine training data for NWVI with threshold from -0.4 to -0.1 with interval of 0.05. The average and standard deviation of nine training data for NWVI is shown in Fig. 38 (d). The highest KSS for NWVI is when using -0.2 with 0.899. Therefore threshold for NWVI is decided to use -0.2.

5.2 Comparison with previous sea fog detection result

While the newly presented improved detection method shows KSS value of 0.74 for test data, the detection result using the previous sea fog detection method shows KSS value of 0.48. The previous detection method used in this study is the daytime detection algorithm presented by Wu and Li (2014). In Wu and Li algorithms, they have derived NDSI with band 6 and 1 when in the improved method used band 5 and 1 for NDSI because there was some manufacturing detectors in Aqua/MODIS band 6. For NDSI, threshold is used to determined a pixel as sea fog/stratus cloud as equation (11). Then standard deviation in the thermal IR channel used threshold value as equation (12). The brightness temperature difference (BTD_{back})test used threshold value as equation (13). The normalized difference near-infrared water vapour index (NWVI) test used threshold value as equation (14).

$$\begin{aligned} &-0.15 < NDSI \leq 0.4, \text{if } 10\% < R_{0.67\mu m} < 30\% \\ &-0.15 < NDSI \leq 0.2, \text{if } R_{0.67\mu m} \geq 30\% \end{aligned} \tag{11}$$

$$\sigma_{IR} \leq 2K \tag{12}$$

$$\begin{aligned} &BTD_{back} \leq 8K, \text{if winter time} \\ &BTD_{back} \leq 4K, \text{if non-winter time} \end{aligned} \tag{13}$$

$$NWVI \leq -0.2 \tag{14}$$

Fig. 35 is the one of the detected example using Wu and Li (2014) method with above threshold. It is showing that the detected result is showing some diagonal lines due to the band 6 and some miss after brightness temperature difference test.

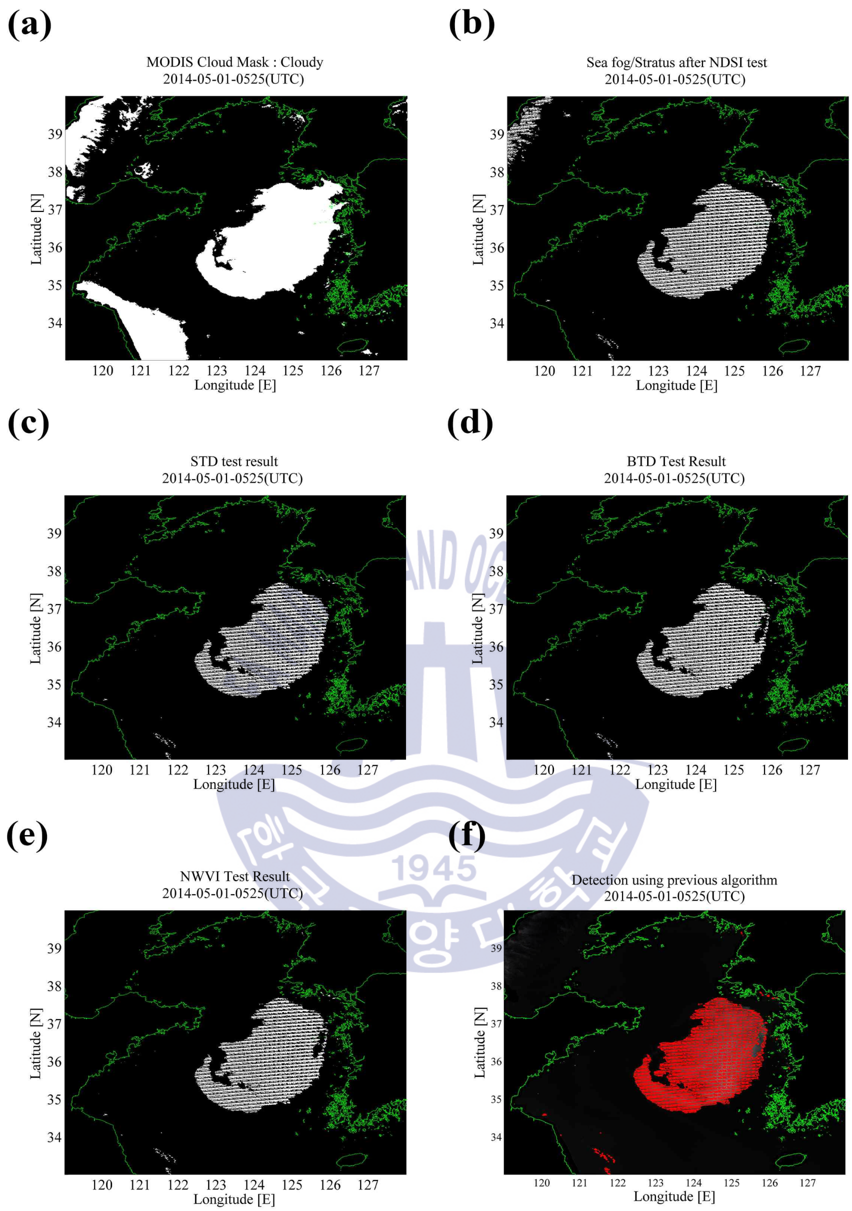

Fig. 35 Result of sea fog detection procedure using Aqua/MODIS on 2014-May-01 05:25 (UTC) through Wu and Li (2014) method. The result after (a) the MODIS Cloud Mask application (Cloudy), (b) the NDSI result, (c) the STD test, (d) the BTD index, (e) the NWVI test, (f) the final sea fog detection result in red closed line on RGB color composite image

Chapter 6. Conclusion

In this study, the new daytime sea fog detection method using MODIS data is developed. The new daytime sea fog detection algorithm shows much better result than the previous algorithms. The main improvements are adjustment of threshold through calculation of KSS. The main difference from the previous result is that it is applicable to both Terra and Aqua MODIS data with new threshold. This new method and threshold are focused to the sea fog event in the Yellow Sea during spring season. The result shows the Hanssen-Kuiper Skill Score of 0.97. It also shows that thin sea fog can also be detected well. However some false detection near the coast line is remained to be solved.

The expected effect of this study is the accuracy improvement of spring season sea fog detection using MODIS data in the Yellow Sea. Further more, with more accurate sea fog detection, it will provide safe information for ship navigation. Based on this preliminary study on spring season daytime sea fog detection method using MODIS data in the Yellow Sea, automatic sea fog detection algorithm can be built after further studies with more cases from other regions and other seasons. For development of sea fog prediction model, the detection result is expected to contribute as their fundamental study.

This detection method is limited to apply for daytime sea fog and the threshold is designed for designated area and season with MODIS data. The MODIS observes the Yellow Sea every two times during the daytime so the temporal resolution is low whereas the temporal changes of sea fog is relatively big.

To solve this problem alternatively for further study, sea fog detection using other sensors based on the current sea fog spectral characteristics is required. Especially, the Geostationary Ocean Color Imagery loaded on the COMS provides eight scenes of daytime for 00:15 to 07:15 (UTC) with interval of one hour. However GOCI only have eight bands of visible and near-infrared. Therefore it is not possible to adapt the current algorithm and method to detect daytime sea fog. If it is possible to detect sea fog using GOCI, it will provide eight scenes every day. Moreover, detecting night time sea fog will be required as well for particularly for merchant ship navigation.

Acknowledgement

2014년 1월 안산에서 시작된 지난 2년 반 동안의 대학원 생활은 지금까지와 전혀 다른 생활이었던 것 같습니다. 처음으로 가족들과 멀리 떨어져 독립적인 생활을 시작하였고 한국해양과학기술원이라고 하는 큰 연구원에 들어오게 되어 설레었던 것도 잠시, 새로운 것들을 배운다고 정신이 없었고 때때로는 외로움을 느낄 새도 없었던 것 같습니다. 많은 도움을 주신 모든 분들께 감사드립니다.

우선 항상 바쁘신 와중에도 잊지 않고 신경 써주신 양찬수 지도 교수님께 감사의 말씀 드립니다. 시작부터 끝까지 많은 관심과 염려를 해주신 덕분에 무사히 석사 과정을 마칠 수 있었던 것 같습니다. 안산까지 오셔서 졸업 심사를 해주신 이은방 교수님께도 감사드립니다. 졸업논문 심사와 더불어 항상 세심하게 지도해주시고 격려해주신 김선화 박사님께도 감사드립니다.

석사 과정 동안 힘들어할 때마다 격려해주시고 많은 조언해주시며 도와주신 정재훈 박사님, 태호 오빠와 단비 언니께도 진심으로 감사드립니다. 항상 늦은 시간까지 함께 연구한 라시드 씨께도 감사드립니다. 대학원 생활 동안 함께 힘들어하고 서로 위로 해가며 동거 동락한 OST 동기 예슬이와 보은이 언니에게도 감사합니다. 그 외에도 많은 위로와 조언으로로 슬럼프를 이기게 해주신 분들, 사랑하는 나의친구들에게도 감사합니다.

마지막으로 무한한 사랑을 주며 응원해준 가족들에게도 감사하다는 말을 전하고싶습니다. 할머니, 부모님 그리고 내 동생 지호 모두 정말 고맙고 사랑합니다. 모두 건강하고 행복해집시다! 사랑합니다♥

Reference

Ackerman, S., Frey, R., Strabala, K., Liu, Y., Gumley, L., Baum, B. and Menzel, P. (2010). Discriminating Clear-Sky from Cloud with MODIS, Algorithm Theoretical Basis Document (MOD35), Version 6.1. Washington DC: NASA. Available at: http://modis-atmos.gsfc.nasa.gov/_docs/MOD35_ATBD_Collection6.pdf[Accessed 31 Mar. 2016].

Ackerman, S., Strabala, K., Menzel, W., Frey, R., Moeller, C. and Gumley, L. (1998). Discriminating Clear Sky from Clouds with MODIS. Journal of Geophysical Research: Atmospheres, 103(D24), pp.32141-32157.

Ahn, M., Sohn, E. and Hwang, B. (2003). A New Algorithm for Sea Fog/Stratus Detection Using GMS-5 IR Data. Advances in Atmospheric Sciences, 20(6), pp.899-913.

Bendix, J. (2002). A Satellite-Based Climatology of Fog and Low-Level Stratus in Germany and Adjacent Areas. Atmospheric Research, 64(1-4), pp.3-18.

Bendix, J., Thies, B., Cermak, J. and Nauß, T. (2005). Ground Fog Detection from Space Based on MODIS Daytime Data—A Feasibility Study. Weather Forecasting, 20(6), pp.989-1005.

Bendix, J., Thies, B., Nauß, T. and Cermak, J. (2006). A Feasibility Study of Daytime Fog and Low Stratus Detection with TERRA/AQUA-MODIS over Land. Meteorological Applications, 13(02), pp.111-125.

Cermak, J. and Bendix, J. (2007). Dynamical Nighttime Fog/Low Stratus Detection Based on Meteosat SEVIRI Data: A Feasibility Study. Pure and Applied Geophysics, 164(6-7), pp.1179-1192.

Cermak, J. and Bendix, J. (2008). A Novel Approach to Fog/Low Stratus Detection Using Meteosat 8 Data. Atmospheric Research, 87(3-4), pp.279-292.

Cermak, J. and Bendix, J. (2011). Detecting Ground Fog from Space – a Microphysics-Based Approach. International Journal of Remote Sensing, 32(12), pp.3345-3371.

Cho, Y., Kim, M. and Kim, B. (2000). Sea Fog around the Korean Peninsula. Journal of Applied Meteorology, 39(12), pp.2473-2479.

Dozier, J. (1989). Spectral Signature of Alpine Snow Cover from the Landsat Thematic Mapper. Remote Sensing of Environment, 28, pp.9-22.

Dozier, J. and Painter, T. (2004). Multispectral and Hyperspectral Remote Sensing of Alpine Snow Properties. Annual Review of Earth and Planetary Sciences, 32(1), pp.465-494.

Ellrod, G. (1995). Advances in the Detection and Analysis of Fog at Night Using GOES Multispectral Infrared Imagery. Weather Forecasting, 10(3), pp.606-619.

Eyre, J., Brownscombe, J. and Allam, R. (1984). Detection of Fog at Night Using Advanced Very High Resolution Radiometer (AVHRR) Imagery. Meteorological Magazine, 113, pp.265-271.

Fu, G., Guo, J., Xie, S., Duan, Y. and Zhang, M. (2006). Analysis and High-Resolution Modeling of a Dense Sea Fog Event over the Yellow Sea. Atmospheric Research, 81(4), pp.293-303.

Gao, S., Wu, W., Zhu, L., Fu, G. and Huang, B. (2009). Detection of Nighttime Sea Fog/Stratus over the Huanghai Sea Using MTSAT-1R IR Data. Acta Oceanologica Sinica, 28(2), pp.23-35.

Gultepe, I., Tardif, R., Michaelides, S., Cermak, J., Bott, A., Bendix, J., Müller, M., Pagowski, M., Hansen, B., Ellrod, G., Jacobs, W., Toth, G. and Cober, S. (2007). Fog Research: A Review of Past Achievements and Future Perspectives. Pure and Applied Geophysics, 164(6-7), pp.1121-1159.

Hall, D. and Riggs, G. (2011). Normalized-Difference Snow Index (NDSI). In: Encyclopedia of Snow, Ice and Glaciers, 1st ed. pp.779-780.

Hao, Z., Pan, D., Gong, F. and Chen, J. (2009). Sea Fog Characteristics Based on MODIS Data and Streamer Model. [online] Available at: http://dx.doi.org/10.1117/12.829949 [Accessed 31 May 2015].

Heo, K. and Ha, K. (2004). Classification of Synoptic Pattern Associated with Coastal Fog around the Korean Peninsula. Asia-Pacific Journal of Atmospheric Sciences, 40(5), pp.541-556.

Heo, K. and Ha, K. (2010). A Coupled Model Study on the Formation and Dissipation of Sea Fogs. Monthly Weather Review, 138(4), pp.1186-1205.

Heo, K., Kim, J., Shim, J., Ha, K., Suh, A., Oh, H. and Min, S. (2008). A Remote Sensed Data Combined Method for Sea Fog Detection. Korean Journal of Remote Sensing, 24(1), pp.1-16.

Heo, K., Min, S., Ha, K. and Kim, J. (2008). Discrimination between Sea Fog and Low Stratus Using Texture Structure of MODIS Satellite Images. Korean Journal of Remote Sensing, 24(6), pp.571-581.

Heo, K., Park, S., Ha, K. and Shim, J. (2012). Algorithm for Sea Fog Monitoring with the Use of Information Technologies. Meteorological Applications, 21(2), pp.350-359.

Hunt, G. (1973). Radiative Properties of Terrestrial Clouds at Visible and Infra-Red Thermal Window Wavelengths. Quarterly Journal of the Royal Meteorological Society, 99(420), pp.346-369.

Kriebel, K., Gesell, G., Kästner, M. and Mannstein, H. (2003). The Cloud Analysis Tool APOLLO: Improvements and Validations. International Journal of Remote Sensing, 24(12), pp.2389-2408.

Lee, T., Turk, F. and Richardson, K. (1997). Stratus and Fog Products Using

GOES-8-9 3.9-μm Data. Weather Forecasting, 12(3), pp.664-677.

Salomonson, V. and Appel, I. (2004). Estimating Fractional Snow Cover from MODIS Using the Normalized Difference Snow Index. Remote Sensing of Environment, 89(3), pp.351-360.

Stowe, L., Davis, P. and McClain, E. (1999). Scientific Basis and Initial Evaluation of the CLAVR-1 Global Clear/Cloud Classification Algorithm for the Advanced Very High Resolution Radiometer. Journal of Atmospheric and Oceanic Technology, 16(6), pp.656-681.

Turner, J., Allam, R. and Maine, D. (1984). A Case Study of the Detection of Fog at Night Using Channel 3 and 4 on the Advanced Very High Resolution Radiometer (AVHRR). Meteorological Magazine, 115, pp.285-290.

Wang, M. and Shi, W. (2006). Cloud Masking for Ocean Color Data Processing in the Coastal Regions. IEEE Transactions on Geoscience and Remote Sensing, 44(11), pp.3196-3105.

White, D. (2008). The MODIS Conversion Toolkit (MCTK) User's Guide. 1st ed. [ebook] Available at: http://nsidc.org/data/modis/tools.html [Accessed 31 May 2015].

Wu, D., Lu, B., Zhang, T. and Yan, F. (2015). A Method of Detecting Sea Fogs Using CALIOP Data and Its Application to Improve MODIS-Based Sea Fog Detection. Journal of Quantitative Spectroscopy and Radiative Transfer, 153, pp.88-94.

Wu, X. and Li, S. (2014). Automatic Sea Fog Detection over Chinese Adjacent Oceans Using Terra/MODIS Data. International Journal of Remote Sensing, 35(21), pp.7430-7457.

Yang, C., Kim, S., Ouchi, K. and Back, J. (2015). Generation of High Resolution Sea Surface Temperature Using Multi-Satellite Data for Operational Oceanography. Acta Oceanologica Sinica, 34(7), pp.74-88.

Yi, L., Zhang, S., Thies, B., Shi, X., Trachte, K. and Bendix, J. (2015). Spatio-Temporal Detection of Fog and Low Stratus Top Heights over the Yellow Sea with Geostationary Satellite Data as a Precondition for Ground Fog Detection — a Feasibility Study. Atmospheric Research, 151, pp.212-223.

Yoo, J., Kim, Y., Ahn, M., Kim, Y. and Chung, C. (2005). Characteristics of MODIS Satellite Data during Fog Occurrence near the Inchon International Airport. Journal of Korean Earth Science Society, 26(2), pp.149-159.

Zhang, S. and Yi, L. (2013). A Comprehensive Dynamic Threshold Algorithm for Daytime Sea Fog Retrieval over the Chinese Adjacent Seas. Pure and Applied Geophysics, 170(11), pp.1931-1944.

Zhang, S., Li, M., Meng, X., Fu, G., Ren, Z. and Gao, S. (2011). A Comparison Study between Spring and Summer Fogs in the Yellow Sea-Observations and Mechanisms. Pure and Applied Geophysics, 169(5-6), pp.1001-1017.